Structural Characteristics of Lightweight Ferrocement Walls with Various Types of Core Materials and Mesh Reinforcement

Abstract

This research presented the structural characteristics of lightweight ferrocement walls with various types of core materials and mesh reinforcement. Specimens were reinforced with expanded metal mesh, welded wire mesh and tenax SS30 mesh. Ten specimens having cross-sectional dimensions of (80cm *10cm) and height of 100 cm were cast and tested until failure. Structural behavior of studied walls in terms of; first crack load, ultimate load, service load ,ductility ratio and energy absorption were investigated in addition to crack pattern and mode of failure for all tested specimens. Theoretical study will be conducted by finite element software (ABAQUS) to evaluate the experimental results and this theoretical study gave good results comparing with the experimental results. This study revealed that the ultimate load for control (CO) specimen was more than the ultimate load for the other specimens that reinforced with welded wire mesh (W), expanded metal mesh (EX) and tenax SS30 mesh (TE). In addition, using the ultimate load for one layer of expanded steel mesh (EX1) was greater than the ultimate load for specimens that reinforced with one layer of welded wire mesh (W1) and one layer tenax mesh (TE1), as well using two layers of expanded steel mesh (EX2) was greater than specimens that reinforced with two layers of welded wire mesh (W2) and two layers of tenax mesh (TE2). And it was observed that the maximum weight/ load ratio for (CO) and (W4) specimens and the minimum weight/ load ratio for (W1) specimen.

Keywords: ferrocement; light weight; walls; Expanded; Welded; Tenax; FE modelling; ABAQUS.

Introduction

Ferrocement is relatively a new material which consists of cement mortar and wire meshes such as welded wire mesh and expanded wire mesh. This type of concrete has low weight, less shrinkage and better durability than ordinary reinforced concrete.

Ferrocement have applications in all fields of civil construction, including water and soil retaining structures, building components, space structures of large size, bridges, domes, dams, boats, conduits, bunkers, silos, treatment plants for water and sewage.

Ferrocement walls can be pre-cast with cores to minimize self-weight and manufacturing costs. These walls are frequently employed in residential and industrial buildings because of its advantages like as high acoustical and thermal, ease of installation, high quality and fire resistance.

This research presented the structural characteristics of lightweight ferrocement walls with various types of core materials and mesh reinforcement which were reinforced with expanded metal mesh, welded wire mesh and tenax SS30 mesh. Ten specimens having cross-sectional dimensions of (80cm *10cm) and height of 100 cm were cast and tested until failure. Structural behavior of studied walls, strain characteristics, crack pattern and failure mode will be investigated. Theoretical study will be conducted by finite element software (ABAQUS) to evaluate the experimental results.

Shaheen et al. (2016) studied the behavior of reinforced ferrocement lightweight columns by permanent precast lightweight ferrocement hollow blocks and the results showed that an improvement in the cracks resistance, serviceability loads, ultimate loads, and energy absorption. Good agreement was found compared with the experimental results. this paper presents applications of using light weight ferrocement units in construction of low-cost housing which are very useful for developed and developing countries alike with great economic advantages. [1]

Noor A. M. et al. (2006) studied strength and behavior of lightweight ferrocement aerated concrete sandwich blocks. The compressive strength increases with the increase in wire mesh layers, single layer of wire mesh may be considered as optimum in terms of compressive strength, strength and behavior of lightweight ferrocement aerated concrete sandwich blocks. [2]

Shaheen et al. (2015) studied the Flexural Behavior of Lightweight Composite Ferrocement Plates and The test results revealed remarkable enhancement in the flexural behavior and potential application of lightweight ferrocement (LWF) composite plates to produce lightweight structural elements as compared to that of the reinforced concrete (RC) plates, which lead towards the industrialization of building system and meets with innovation and expansible application of concrete construction technology results in better efficiency of developing of lightweight composite ferrocement plates .[3]

Tawab et al. (2012) presented the results of an experi- mental investigation to examine the feasibility and effec- tiveness of using precast U-shaped ferrocement laminates as permanent forms for construction of reinforced concrete beams. The results showed that crack resistance control, high serviceability load, ultimate loads, and good energy absorption properties could be improved using the pro- posed ferrocement forms. [4]

Shaheen et al. (2021) studied the Performance of Ferrocement Box Shear Wall with Webs and The results showed that the structural performance of the ferrocement box shear wall with webs (ribs) is better than those walls without ribs and the ferrocement walls reinforced with double layers of welded wire meshes has better structural behavior than those walls reinforced with expanded wire meshes. [5]

Shaheen et al. (2004) studied ferrocement sandwich and cored panels for floor and wall construction. The sandwich panels consisted of two thin ferrocement layers reinforced with one or two layers of closely spaced welded wire mesh. The core of the panel was made of light weight brick. Steel wires were used to tie the steel meshes of the two skin layers together and to act as shear connectors to transfer shear between the two ferrocement skin layers . These steel wires were embedded in the mortar joints of the brick. The thickness of the ferrocement skin layer was 25mm when single layer of wire mesh was used and 35mm when two layers of mesh reinforcement were used. The core material was 70 mm thick. The results showed that high ultimate and serviceability loads, crack resistance control, high ductility, and good energy absorption properties could be achieved by using the proposed panels. [6]

Mahmoud A. W. and Kimio F. (2010) studied the flexural behavior of lightweight ferrocement sandwich composite beams. There results refer to the LWF beams revealed the remarkable enhancement in the structural behavior and potential application of lightweight sandwich ferrocement polystyrene foam composite as compared to that of the RC beams. This leads to wards the Industrialization of building system and meets with innovation and responsible application of concrete construction technology which results in better efficiency of the composite. [7]

Shaheen et al. (2012) studied the structural behavior of composite reinforced Ferrocement Plates, The cracking loads slightly increased as the reinforcement volume fraction increased. The cracking loads were independent of the mesh type. The flexural capacity of the composite plates increased with the increase of the specific surface area of the mesh. [8]

Experimental program

The experimental program consists of ten specimens according to the mesh type and number of steel mesh layers as shown below.

Wall (1)

Control specimen (CO) which was cast using conventional reinforcement, with steel bars Φ10mm in

each side as shown in Fig.1.

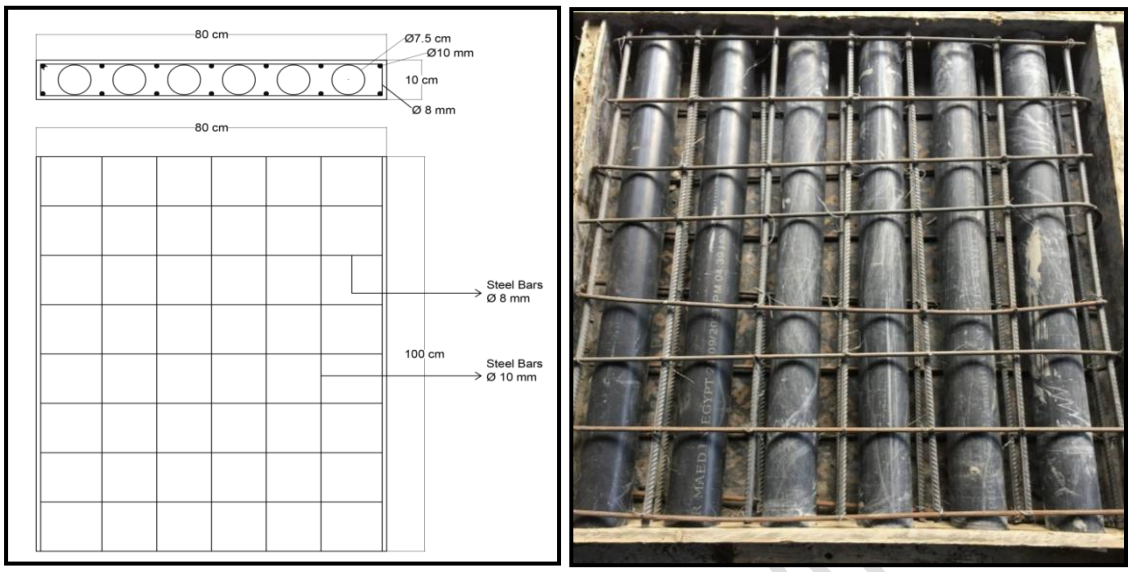

Fig. 1: Control specimen

Wall (2)

This wall was cast using one layer from welded steel wire mesh as shown in Fig.2.

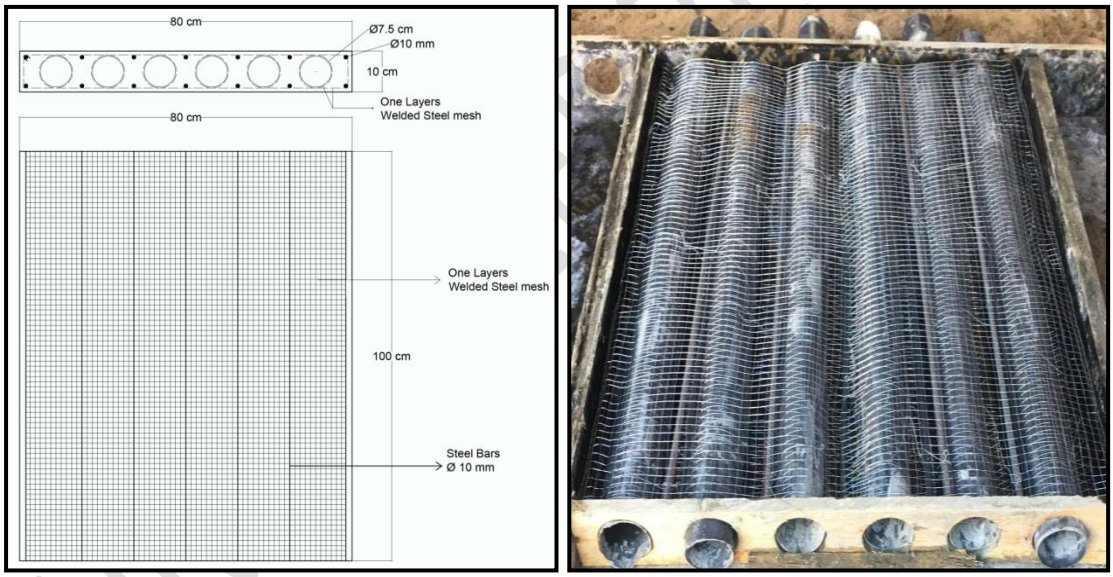

Fig. 2: One layer welded steel mesh specimen

Wall (3)

This wall was cast using two layers from welded steel wire mesh as shown in Fig.3.

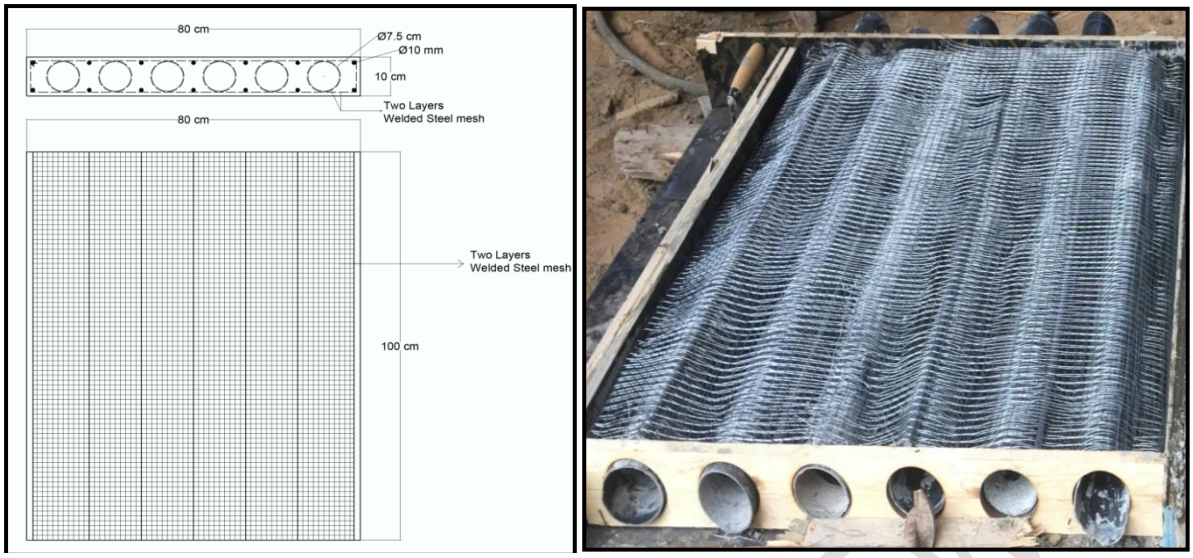

Fig. 3: Two layers welded steel mesh specimen

Wall (4)

This wall was cast using three layers from welded steel wire mesh as shown in Fig.4.

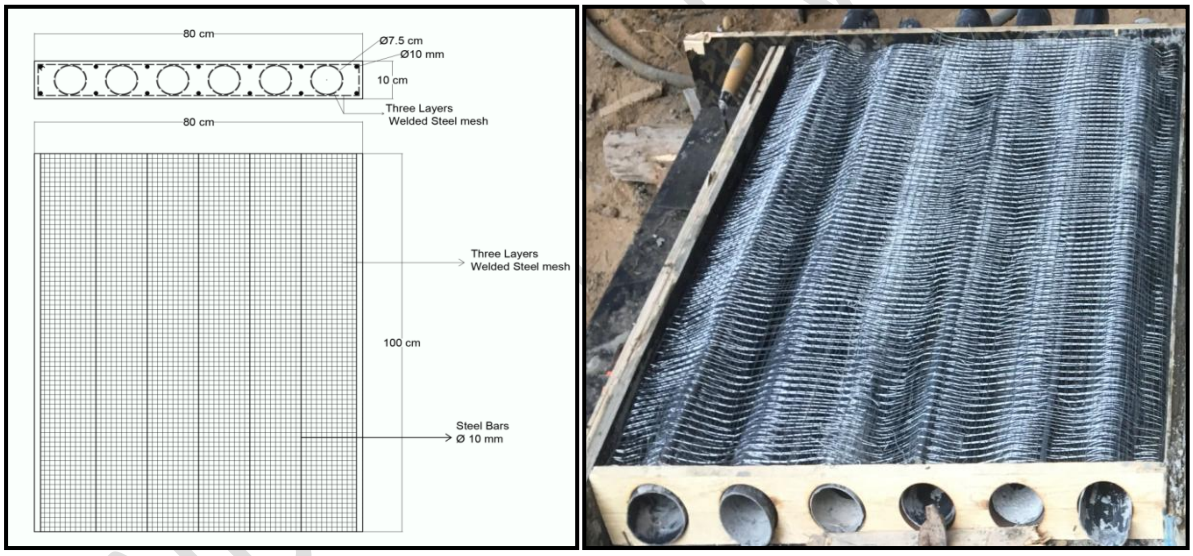

Fig. 4: Three layers welded steel mesh specimen

Wall (5)

This wall was cast using four layers from welded steel wire mesh as shown in Fig.5.

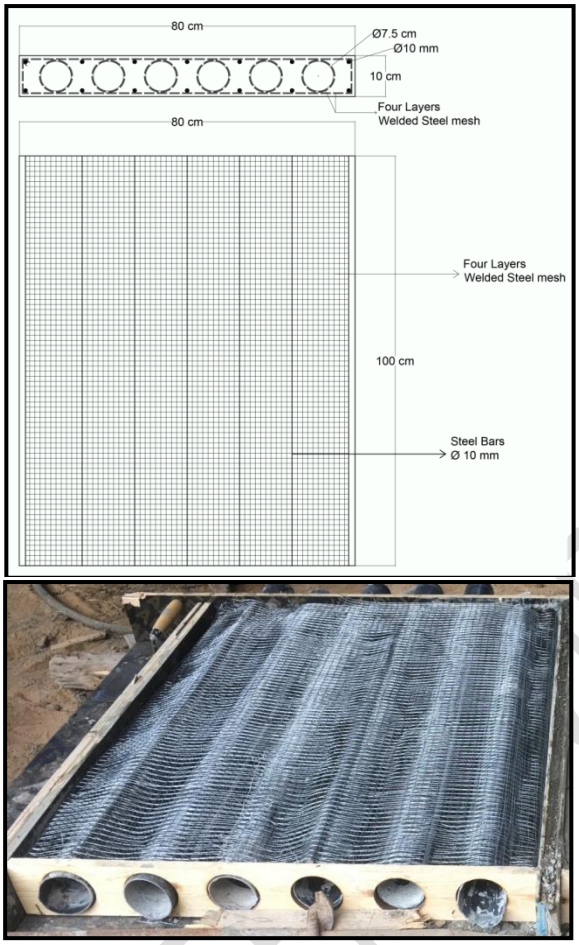

Fig. 5: Four layers welded steel mesh specimen

Wall (6)

This wall was cast using one layer from expanded steel mesh as shown in Fig. 6.

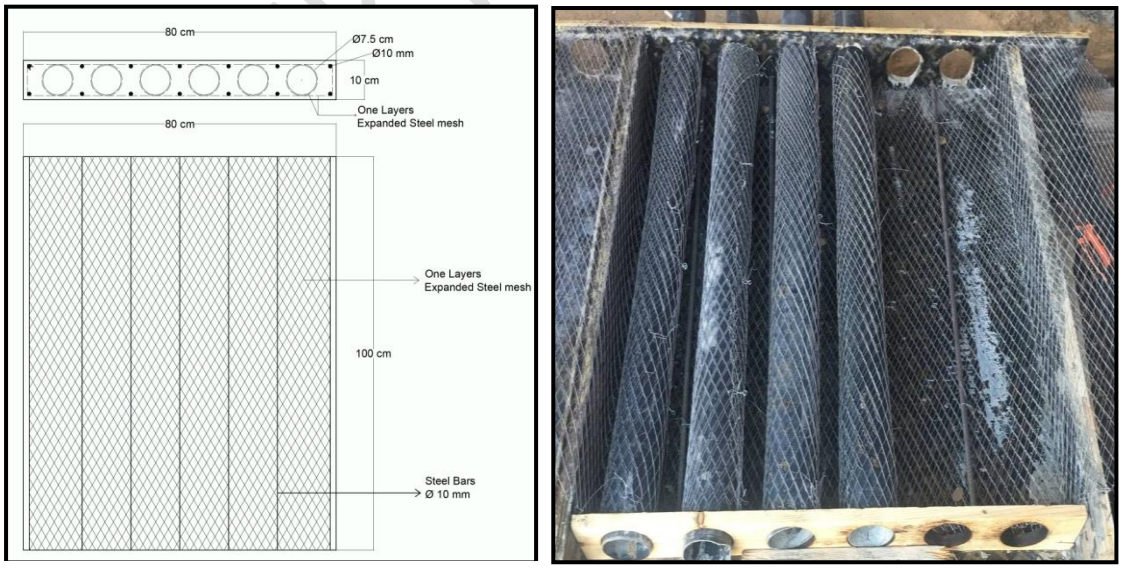

Fig. 6: One layer expanded steel mesh specimen

Wall (7)

This wall was cast using two layers from expanded steel mesh as shown in Fig. 7.

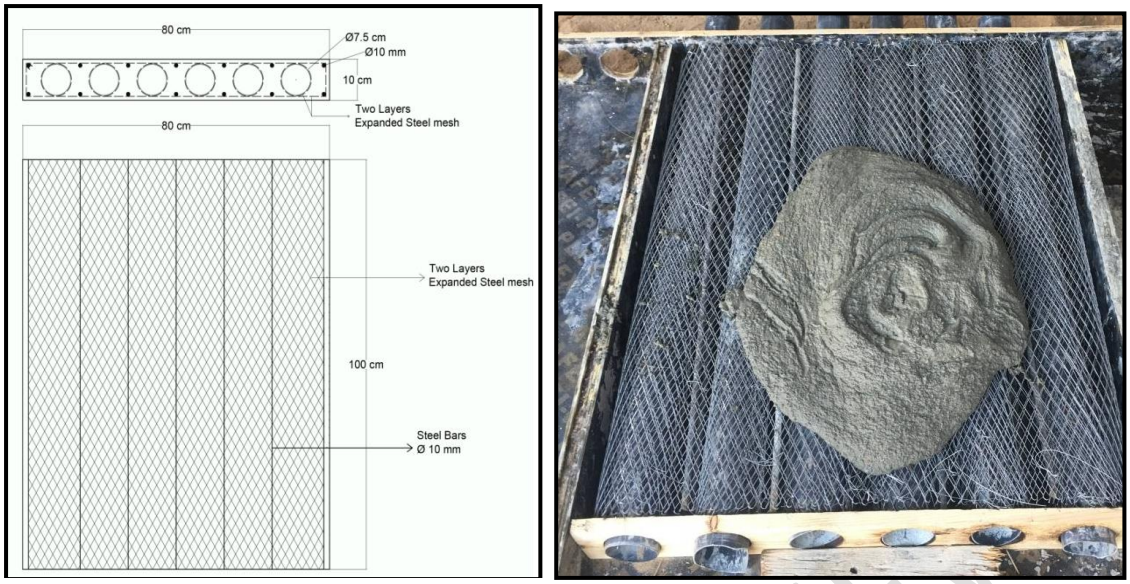

Fig. 7: Two layers expanded steel mesh specimen

Wall (8)

This wall was cast using one layer from tenax mesh as shown in Fig. 8.

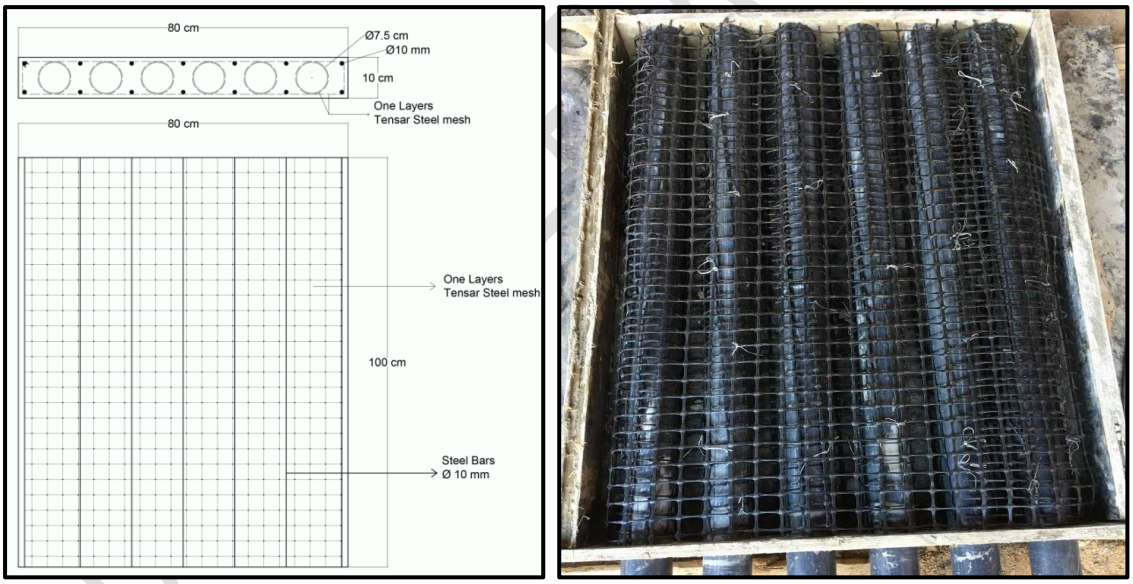

Fig. 8: one layer tenax mesh specimen

Wall (9)

This wall was cast using two layers from tenax mesh as shown in Fig. 9

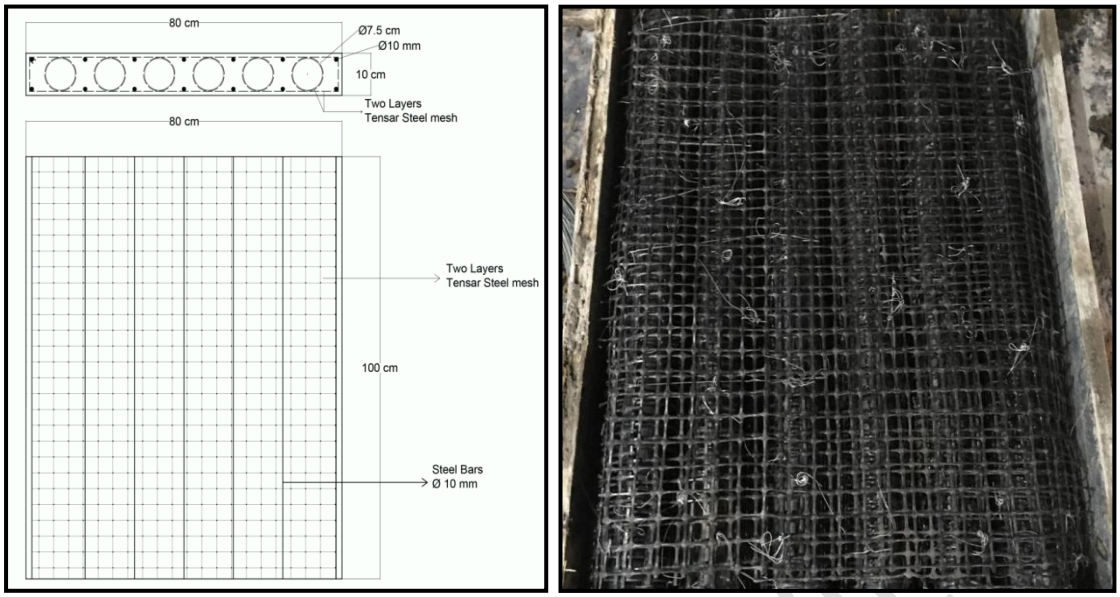

Fig. 9: two layers tenax mesh specimen

Wall (10)

This wall was cast using three layers from tenax mesh as shown in Fig. 10.

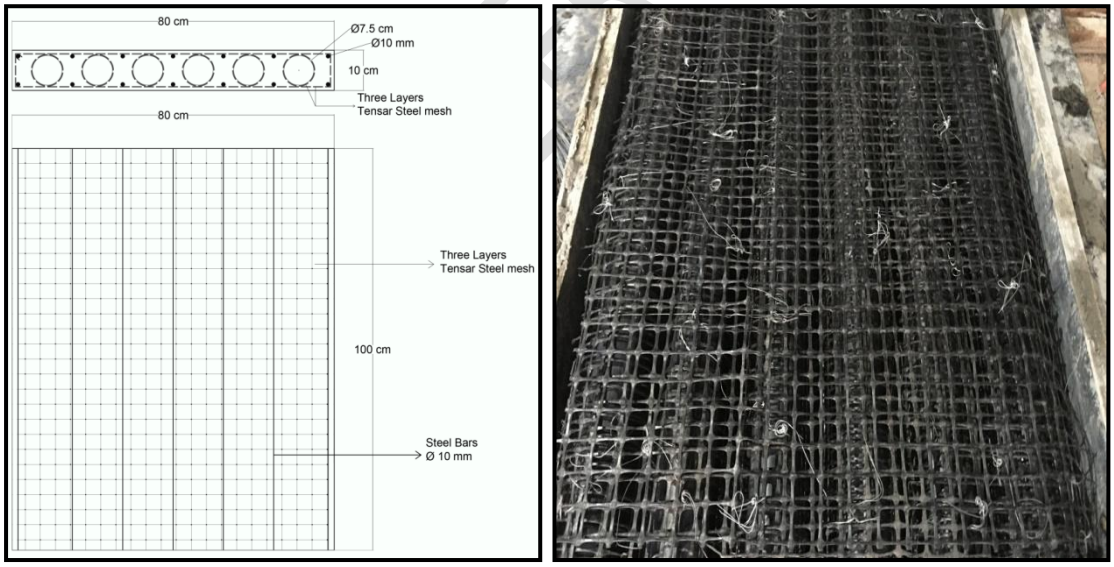

Fig. 10: three layers tenax mesh specimen

Material properties

The properties of materials that used in mortar mix design in addition to the reinforcing steel bars, steel meshes, fibres and the chemical admixtures are given in the following sections.

Cement

Ordinary Portland cement (CEM I 42.5N) was used in all mixes. The chemical analysis of the used cement according to ASTM C114/2013 was shown in Table (1).

Table (1): The chemical analysis of used cement.

Sample ID	% in Cement
SiO2	21.0189
Fe2O3	4.0802
Al2O3	4.9932
CaO	63.0104
MgO	0.8911
P2O5	-
Na2O	0.5129
K2O	0.2152
Cl	0.0311
SO3	2.9167
MnO2	-
L.O.I	2.3144
TOTAL	99.9841
Active SiO2	19.9932
Non-Active	1.0257

Pozzolanic materials

Pozzolanic materials such as Micro Silica fume (MS) and Fly ash (FA) were used as a partial replacement of cement to produce blended mixtures. The FA that used in mixes was Class F (low Calcium) according to ASTM and ACI classifications. The chemical analysis of the used FA according to ASTM C114/2013 was shown in Table (2). Micro silica fume (MS) which used in this research was Rheomac SF 100 densified silica fume which meets the requirements of ASTM C 1240. The chemical analysis of the used MS according to ASTM C114/2013 was shown in Table (3).

Water

Potable water that was free from impurities was used for mixing and curing of the test specimens.

Chemical admixtures

Chemical admixture that used in all mixes was Super Plasticizer and High Range Water Reducing admixture (SP) “Sikament 163M” and used to achieve the desired fairly constant workability in all mortar mixtures.

Table (2): The chemical analysis of used Fly Ash

Sample ID	% in Fly Ash
SiO2	58.6393
Fe2O3	7.8524
Al2O3	25.7711
CaO	4.9531
MgO	1.0009
P2O5	0.0547
Na2O	0.8963
K2O	0.2147
Cl	0.0105
SO3	0.0901
MnO2	0.0089
L.O.I	0.4631
TOTAL	99.9547
Active SiO2	31.1587
Non-Active	27.4806

Table (3): The chemical analysis of used Micro Silica

Sample ID	% in Micro Silica
SiO2	95.9962
Fe2O3	0.0862
Al2O3	0.7954
CaO	0.6522
MgO	0.0913
P2O5	0.0082
Na2O	0.4387
K2O	0.0222
Cl	0.0113
SO3	0.0217
MnO2	Nil
L.O.I	1.84
TOTAL	99.9634
Active SiO2	25.7333
Non-Active	70.2629

Aggregate

Fine aggregate that used in this research is sand which passing from sieve No. 4.75 mm and used in saturated surface dry condition. The used aggregate has specific gravity of 2.6, fineness modulus of 2.47 and complied with the limits of ECP 203-2007. Fig. (11) shows the grain size distribution curve of the used sand and ECP 203-2007 limits.

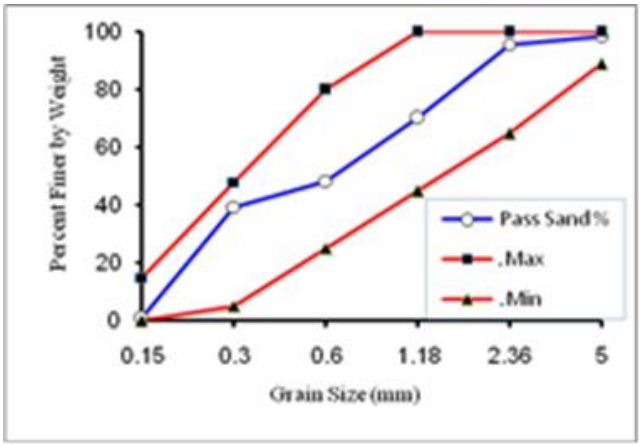

Fig. (11): Grain size distribution of used sand and ECP 203-2007 limits.

Fibers

Synthetic fibers "Fibremesh e 300" as shown in Fig. (3.3) was added to all mortar mixes with 1200 gm/m^3. The Chemical and physical properties of fiber mesh e300 are shown in Table (4).

Table (4): Chemical and Physical Properties of Fiber mesh e 300.

Specific Gravity	0.91
Fiber Length	single cut lengths
Electrical Conductivity	Low
Acid & Salt Resistance	High
Melt Point	324°F (162°C)
Thermal Conductivity	Low
Ignition Point	1100°F (593°C)
Alkali Resistance	Alkali Proof

Reinforcing Steel Bars

High tensile deformed steel bars with diameter of 10 mm were used to reinforce all test specimens. Tensile tests were performed on three samples of the bars as shown in Fig. (12). The average proof stress and ultimate strength for the three samples of the material were 551 MPa and 670 MPa respectively. Mild steel stirrups that used in specimen of diameter 8 mm were used for the control wall only.

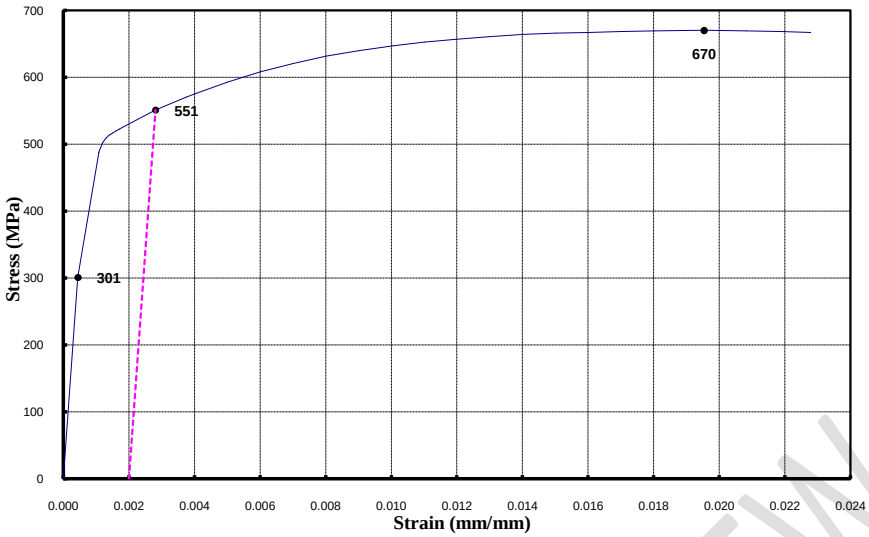

Fig. (12): Stress-strain curve for high tensile steel bars.

In this research , two different steel meshes such as expanded wire mesh and welded wire mesh were used to reinforce the two thin skin layers of each specimen

Expanded steel mesh

Expanded steel mesh with weight equal 1500 gm/m^2, diamond size 31×16.5 mm and thickness of 1.25 mm was used as reinforcing material as shown in Fig. (13) (a). To investigate the mechanical properties of mesh three samples were tested using the Universal Testing Machine. The mesh has ultimate strength of 350 MPa, proof stress of 250 MPa and modulus of elasticity 120 GPa. Table (5) shows the properties of the used steel mesh.

Welded steel mesh

Welded galvanized steel mesh with weight equal 450 gm/m^2 and dimensions of 12.5 mm×12.5 mm was used as shown in Fig. (13) (b). To investigate the mechanical properties of mesh three samples were tested using the Universal Testing Machine. The mesh has ultimate strength of 600 MPa, proof stress of 400 MPa and modulus of elasticity 170 GPa. Table (5) shows the properties of the used steel mesh.

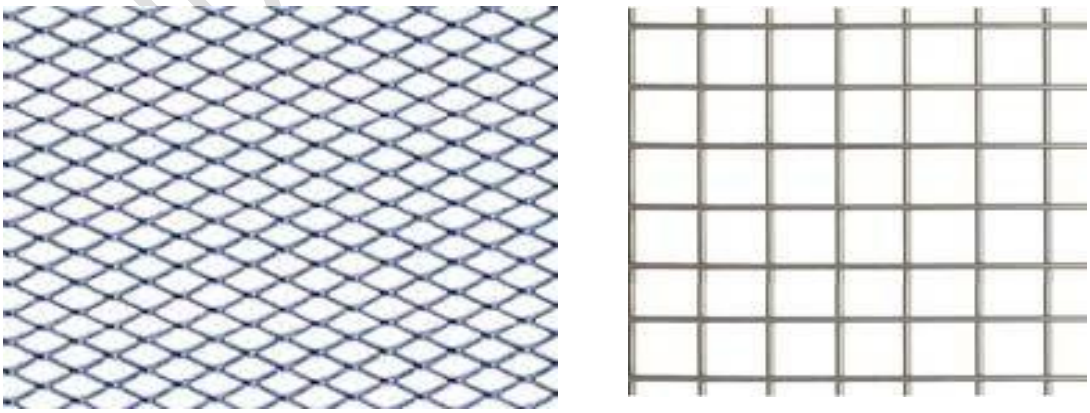

a) Expanded steel mesh b) welded steel mesh

Fig. (13): Types of the steel mesh used.

Table (5): Properties the tested steel meshes

Mesh type	Expanded Metal Mesh	Welded Metal Mesh
Opening Size	diamond size 16*31 mm	dimensions size12.5*12.5 mm
Weight	1.25 kg/m2	430 g/m2
Modulus Of Elasticity	120 GPa.	170 GPa
Proof Stress	199 MPa	400 MPa
Proof Strain	9.7×10-3	1.17×10-3
Ultimate Strength	320 MPa	600 MPa
Ultimate Strain	59.2×10-3	58.8×10-3

Tenax SS30

Tenax geogrids are stiff monolithic geogrids with integral junctions. They are orientated in two directions such that the resulting ribs have a high degree of molecular orientation which continues through the area of the integral node. The ribs have a rectangular cross section with square edges as shown in Fig.(14). Table (6) shows the physical properties of Tenax SS30.

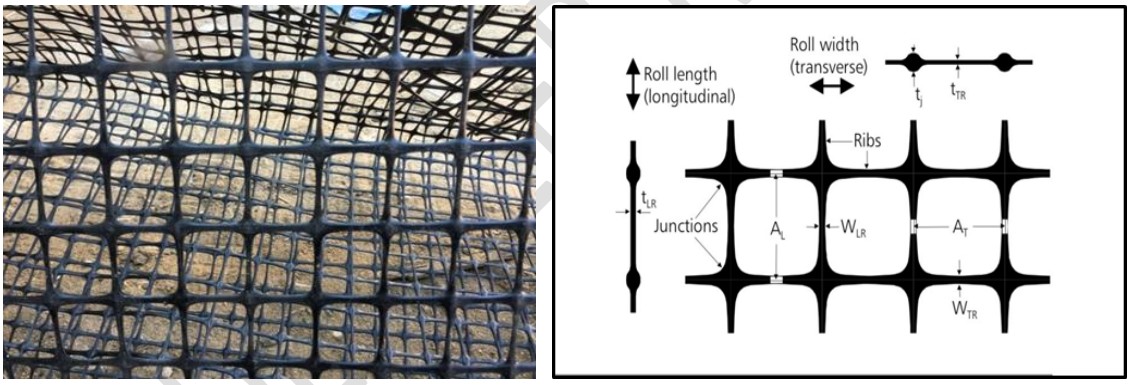

Fig. (14): Tenax SS30 mesh.

Table (6): Physical properties of Tensar SS30.

Structure	Biaxial geogrid
Mesh type	Rectangular apertures
Standard color	Black
Polymer type	Polypropylene
Min. Carbon black content	2%
Aperture size AL	39 mm
Aperture size AT	39 mm
Dimension (W.LR)	2.3 mm
Dimension (W.TR)	2.8 mm
Roll width	4 m
Roll length	50 m
Roll diameter	.52 m
Unit weight	0.33 kg/m2
Roll weight	67 kg

Mortar mix design

The experimental program of this research was designed for producing the Ferrocement walls with light weight of core material by using mortar mix. The mortar mix was designed according to the ACI recommendations. Table (7) shows the quantity of component by weight per cubic meter.

Table (7): Mix design of the ferrocement mortar mix.

	Binder = 680.88 kg/m^3							
Component	**Cement**	**Silica Fume**	**Fly Ash**	**Nano silica sand**	**Fine aggregate**	**Water**	**Super plasticizer**	**e-300**
Amount ((kg/m3)	442.5	68.08	136.16	34.04	1361.77	238.3	13.62	1.2

- **Binder** is the mixture of cement in addition to pozzolanic materials (i.e. MS, FA and Nano silica sand).
- **Silica Fume** = containing 10% replacement of binder content.
- **Fly Ash** = containing 20% replacement of binder content.
- **Nano Silica Sand** = containing 5 % replacement of binder content.
- **Super plasticizer =** 2 % of binder content.

Test Setup

After 28 days from casting, the walls were painted with white paint to make the appearance of cracks easier during testing process. Flexural testing machine of 3500 KN capacities was used. Three Linear Variable Differential Transformers (LVDT) were set on three different points of the test specimen to measure the horizontal and vertical displacement versus load during the test. Ten specimens were tested under compression loadings applied incrementally till failure. The values of deformation characteristics, cracking shape and values of strengths were measured at all stages of loadings. The specimens were loaded at two points through a loading steel beam. The values of deflections at variable positions were recoded and stored using an automatic data logger unit (TDS-150). Fig.(15) shows LVDT sensors, data logger unit and test set up for specimen.

Fig.(15): LVDT sensors, data logger unit and test set up for specimen.

Experimental Results and Discussion

Table (8) shows the first crack load, serviceability load, ultimate load, ductility ratio, and energy absorption for all tested specimens. The serviceability load is defined as the load corresponding to a deflection equal to the height divided by (constant=180) according to the Egyptian code for concrete structures. The ductility ratio is defined here as the ratio between the mid span displacement at ultimate load to that at the first crack load (Δu/Δy). The energy absorption is defined as the total area beneath the load–deflection curve. The area under curve was calculated using a Microsoft office (excel sheet) by integrating the equation of the load–deflection curve for each sample as follows: ultimate load Energy absorbed = $\int_0^{\Delta u} f(\Delta)d\Delta;$ where f (Δ) is the equation of load–deflection curve, and Δu is the mid-span deflection at failure load. Fig. (16) shows the first crack load, ultimate load and serviceability load for all tested specimens. Fig. (17, 18) show the ductility ratio and energy absorption respectively.

Table (8): Test results for all experimental test specimens.

Specimens	First Crack load (kN)	Serviceability Load (kN)	Ultimate Load (kN)	First Crack Displacement (mm)	Maximum displacement (mm)	Ductility Ratio	Energy Absorption (kN.mm)
CO	1725.84	1133.7	1814.58	1.54	1.78	1.15	1718.47
W1	946.05	683.1	1092.93	1.31	1.53	1.16	856.07
W2	991.16	825.6	1320.93	1.18	2.29	1.94	1889.48
W3	1132.20	963.7	1542.75	1.58	2.44	1.54	2208.98
W4	1276.02	1106.8	1771.23	1.84	2.57	1.39	2257.80
EX1	916.30	811.2	1298.11	1.18	1.76	1.49	1193.36
EX2	1120.47	922.5	1475.96	1.11	1.84	1.65	1568.88
TE1	723.69	799.4	1279.59	0.781	1.77	2.27	1275.70
TE2	884.85	858.7	1374.45	1.01	1.98	1.96	1526.38
TE3	920.20	880.6	1409.23	1.23	2.78	2.26	2553.11

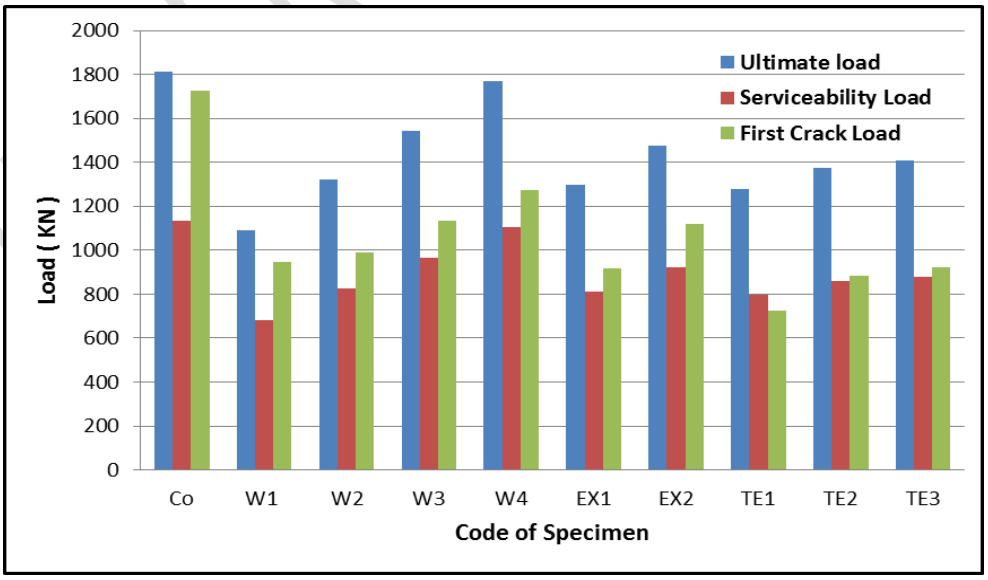

Fig. (16): The first crack load, Ultimate load and Serviceability load for all tested specimens.

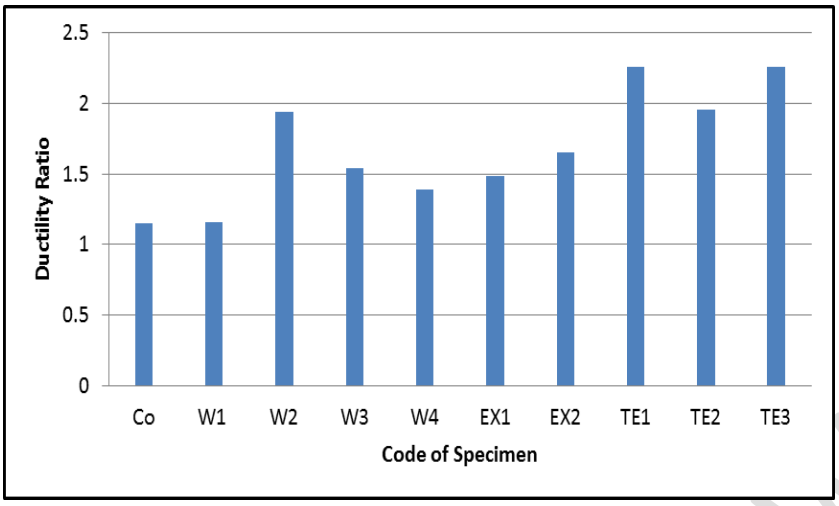

Fig. (17): Ductility Ratio for all tested specimens.

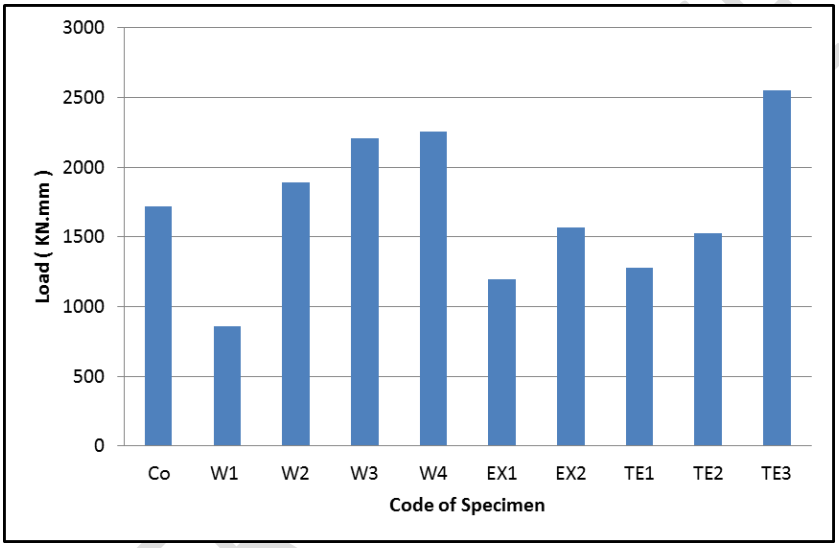

Fig. (18): Energy Absorption of all tested specimens**.**

Behavior of the Test Specimens

Load -Vertical displacement relationships

Fig.(19) shows the load-vertical displacement of the control specimen (CO) and welded wire mesh specimens (W1 , W2 , W3) and from this figure the ultimate load for specimen (CO) is more than that of the specimens (W1 , W2 , W3 , W4) and the percentage of increasing in the ultimate load was 39.7 % , 27.2 % , 14.9% and 2.4% respectively and the ultimate load for specimen (W4) is more than that of the (W1, W2 , W3) specimens by 38.2% , 25.4 % and 12.9 % respectively. This is due to increasing the number of layers. From fig. (20), the ultimate load for specimen (CO) is more than that of the specimens EX1 and EX2 and the percentage of increasing in the ultimate load are 28.4 % and 18.6 % respectively and the ultimate load for specimen (EX2) is more than that of the (EX1) specimen by 12 %. This is due to increasing the number of layers. From fig. (21) the ultimate load for specimen (T3) is more than that of specimen (T1 and T2). This is due to increasing the number of layers and the percentage of increasing in the ultimate load is 9.2 % and 2.4 % respectively. And the ultimate load for specimen (CO) is more than that of the specimens (T1, T2, T3) by 29.5 %, 24.2 % and 22.3 % respectively. Fig. (22) shows the load-vertical displacement for all tested specimens.

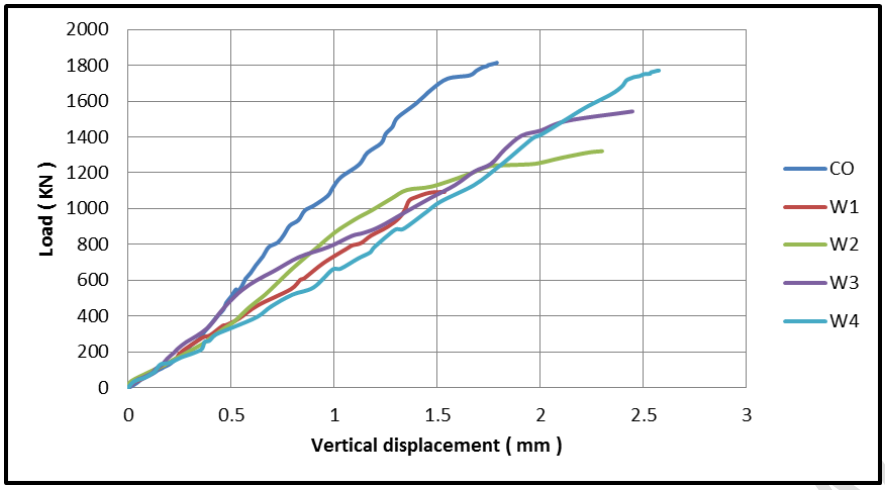

Fig. (19): Load- vertical displacement relationship for control and welded wire mesh specimens.

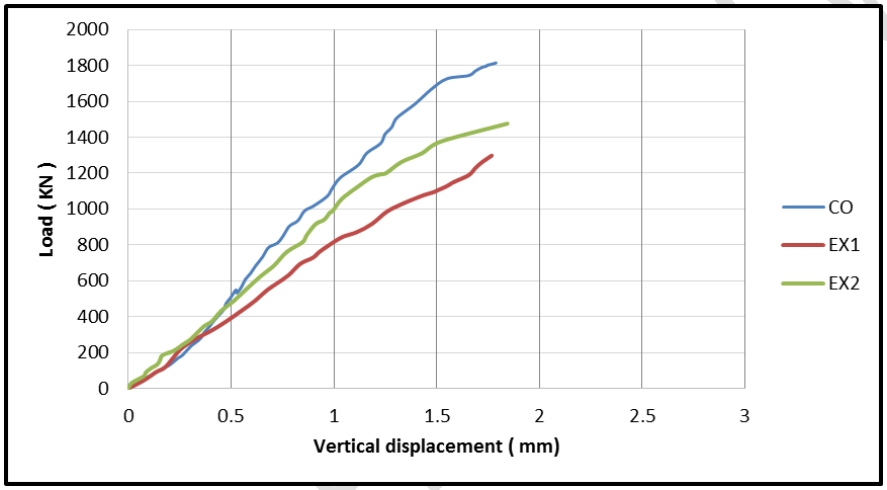

Fig. (20): Load- vertical displacement relationship for control and expanded mesh specimens.

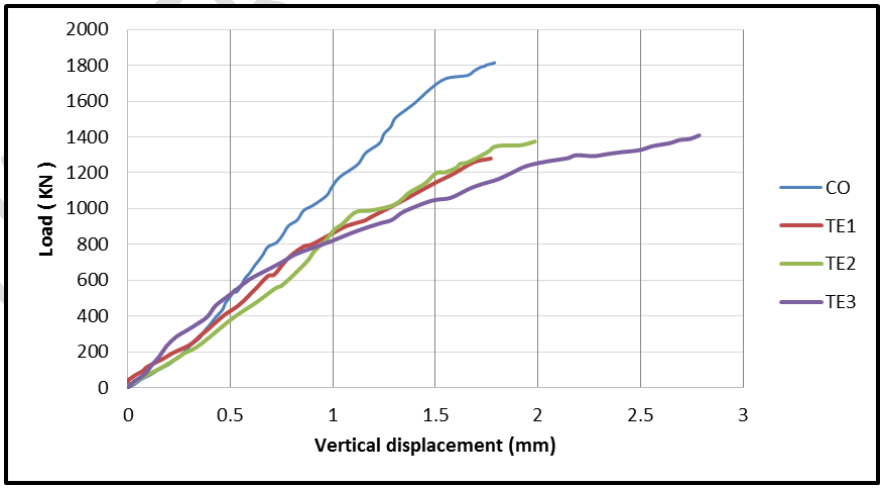

Fig. (21): Load- vertical displacement relationship for control and tenax mesh specimens.

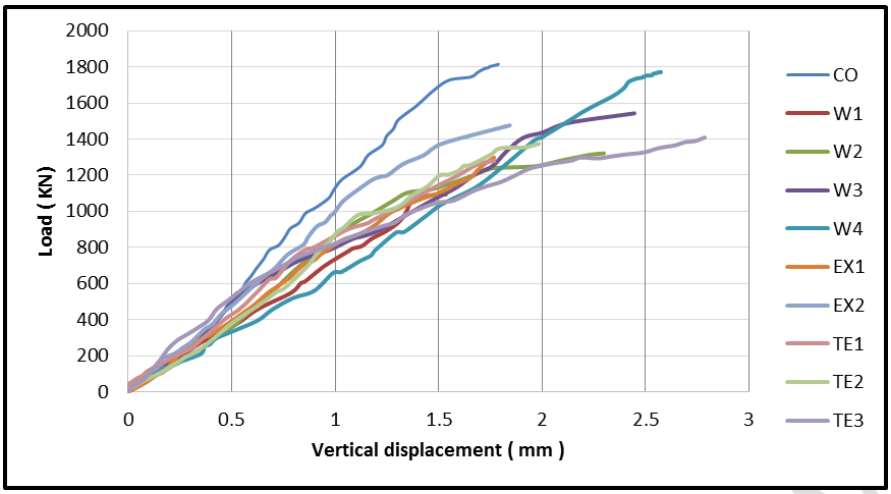

Fig. (22): Load- vertical displacement relationship for all tested specimens.

The Effect of Using Various Types of Meshes

In order to evaluate the effect of using various types of meshes, control specimen was compared to specimens reinforced with welded wire mesh, expanded steel mesh and tenax mesh at the same number of layers. Fig. (23) illustrates the load-displacement curves of the control specimen (CO) that compared to the specimens reinforced with one layer of welded wire mesh (W1),one layer of expanded steel mesh (EX1) and one layer of tenax mesh (TE1). And From this figure the ultimate load for specimen (CO) is more than that of (W1, EX1 and TE1). This is due to the strength of steel bars than any other used meshes in this research. The percentage of increasing in the ultimate load is 39.7%, 28.4% and 29.5% respectively. And the ultimate load for specimen that reinforced with one layer expanded steel mesh EX1 was greater that specimens that reinforced with one layer welded wire mesh W1 and one layer tenax mesh TE1 and the percentage of increasing in ultimate load was 15.8% and 1.4% this is due to the strength of expanded steel mesh. Fig. (24) illustrates the load-displacement curves of the control specimen (CO) that compared to the specimens reinforced with two layers of welded wire mesh (W2),two layers of expanded steel mesh (EX2) and two layers of tenax mesh (TE2). And From this figure the ultimate load for specimen (CO) is more than that of (W2, EX2 and TE2). This is due to the strength of steel bars than any other used meshes in this research. The percentage of increasing in the ultimate load is 27.2%, 18.6% and 24.2% respectively. And the ultimate load for specimen that reinforced with two layers of expanded steel mesh EX2 was greater that specimens that reinforced with two layers of welded wire mesh W2 and two layers of tenax mesh TE2 and the percentage of increasing in ultimate load was 10.5% and 6.9% this is due to the strength of expanded steel mesh.

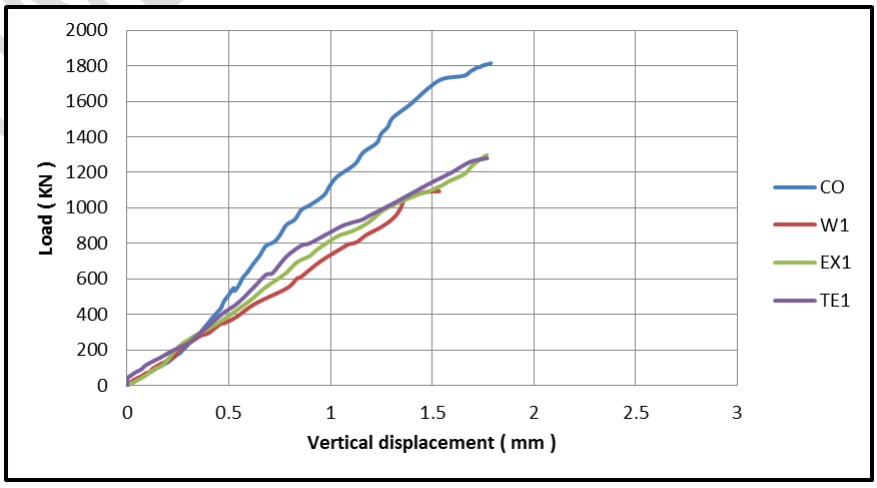

Fig. (23): The effect of type of reinforcement on the load–displacement curves for the specimens.

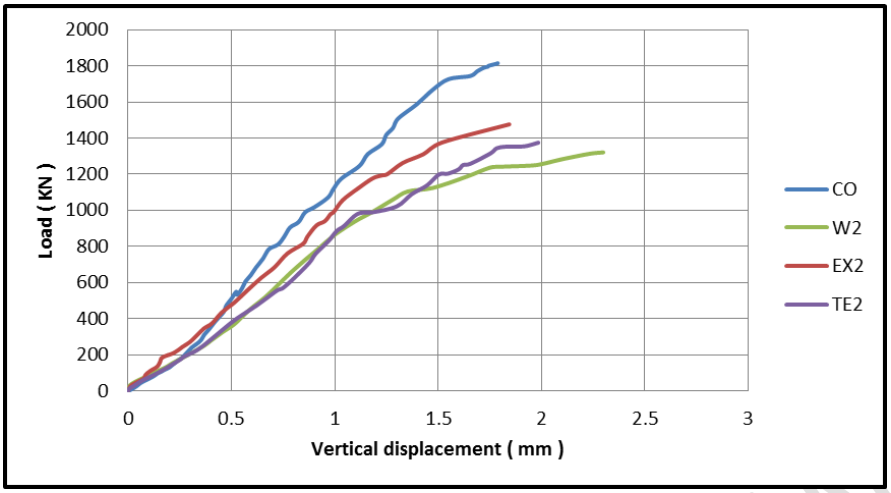

Fig. (24): The effect of type of reinforcement on the load–displacement curves for the specimens.

Load to weight ratio for all tested specimen

Table (9) shows the load to weight ratio for all tested specimen, it was observed from this table that the maximum weight/ load ratio for (CO) and (W4) specimens and the minimum weight/ load ratio for (W1) specimen as shown in fig (25).

Table (9): Load/ weight for all experimental test specimens

Specimen	Load	Weight	Load / Weight
CO	1814.58	166	10.93
W1	1092.93	162.75	6.71
W2	1320.93	163.5	8.07
W3	1542.75	164.25	9.39
W4	1771.23	165	10.73
EX1	1298.11	164.83	7.87
EX2	1475.96	167.66	8.80
TE1	1279.59	158	8.09
TE2	1374.45	158.66	8.66
TE3	1409.23	159.5	8.83

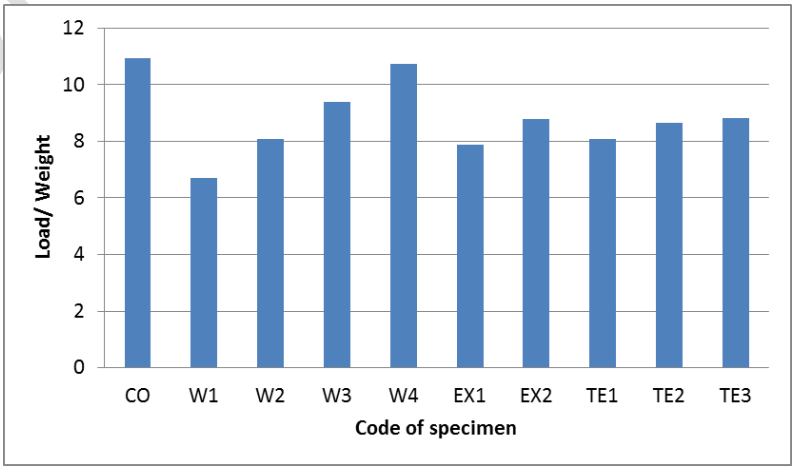

Fig. (25): Load/ weight for all tested specimens.

Cracking Patterns and Mode of Failure

Cracks were started to appear by increasing in loading. The cracks generated and progressed vertically by increasing in loading. When the specimens reached to their failure load, the cracks began to propagate wider. Cracks were traced and marked over the specimen's sides. Cracks propagation and modes of failure for each specimen were recorded as shown in Fig.(26).

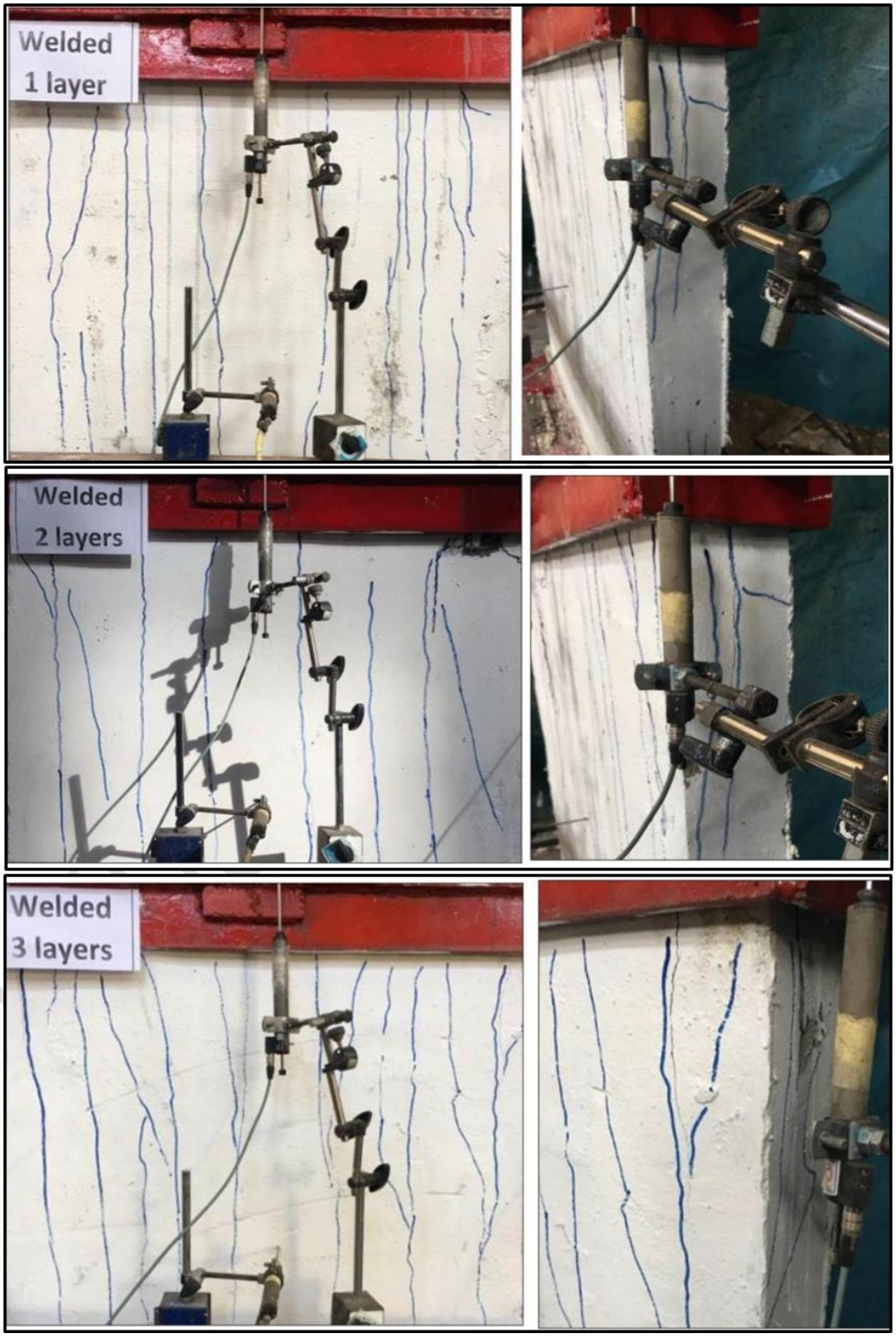


Welded
4 layers


Expanded
1 layer


Expanded
2 layers
Expanded
2 layers

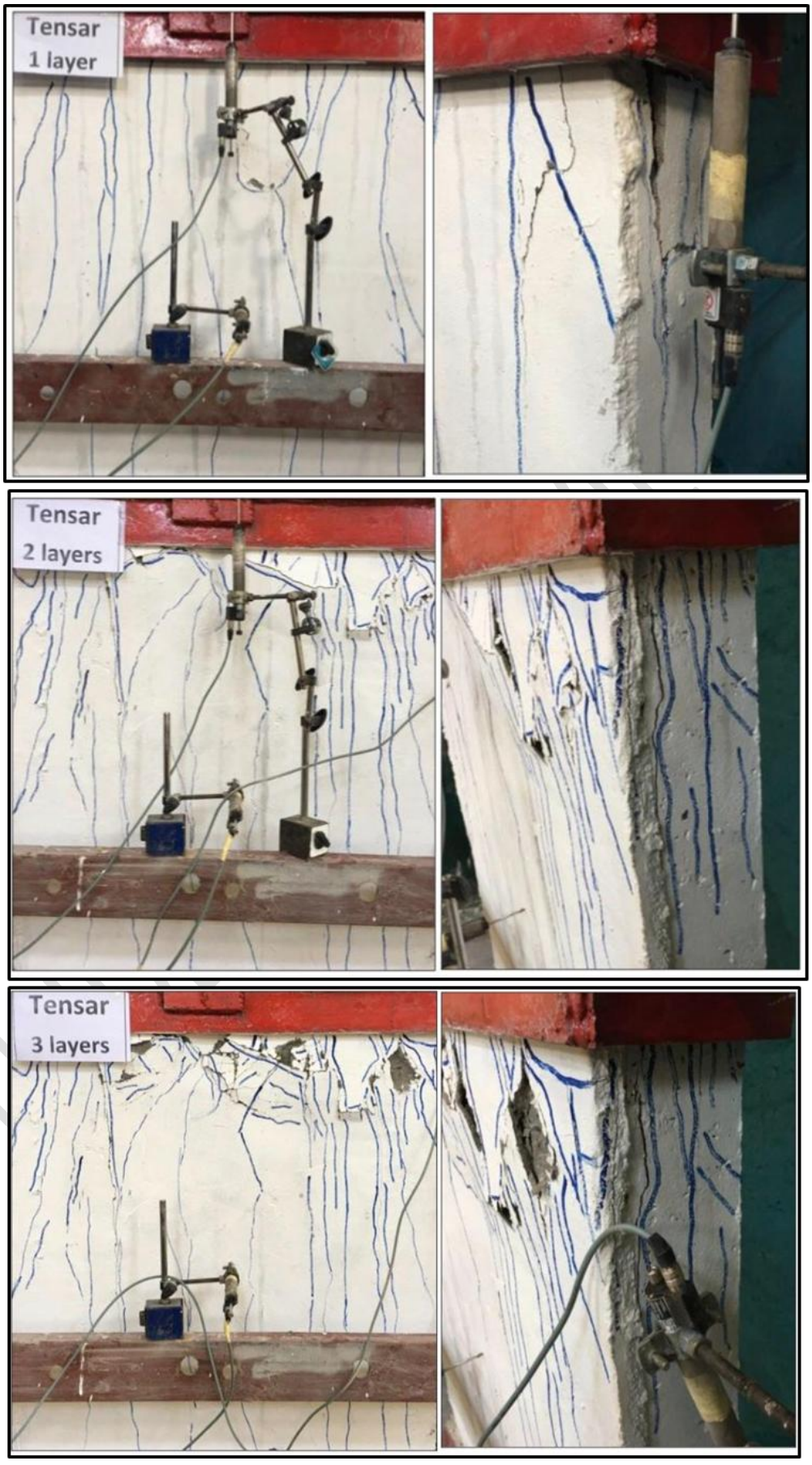

Fig. (26): Cracks propagation for each specimen.

Finite element simulation

In order to get a more in-depth understanding of Structural behavior of Lightweight Ferrocement Walls, Finite element (FE) model was developed to simulate the different specimens. In this study Abaqus was used for analysis. Abaqus is a multi-purpose analysis product that uses a standard static FE formulation. It is suitable for modeling uniform static pressures, ramping loading, and nonlinear problems involving changing contact conditions, such as forming simulations [9].

The specimens of current study were modeled as 3D structures. Concrete parts were modeled as a solid element using C3D8R. Steel bars, welded and expanded steel meshes were modeled using truss element T3D2 elements. Tenax mesh was modeled as a shell element. Fig. (19) shows modeling of all parts (concrete , adipor, loading plate, Steel bars, welded, expanded and tenax meshes) in Abaqus.

Modeling of steel bars

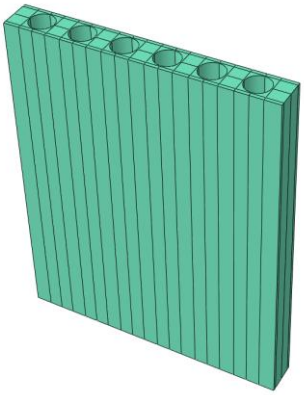

Modeling of concrete part

Modeling of adipor part

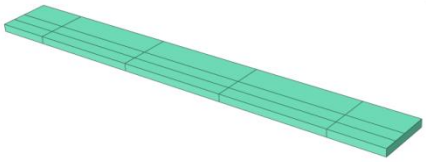

Modeling of loading plate

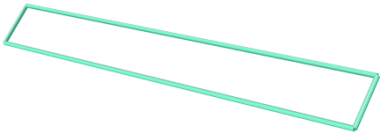

Modeling of stirrups

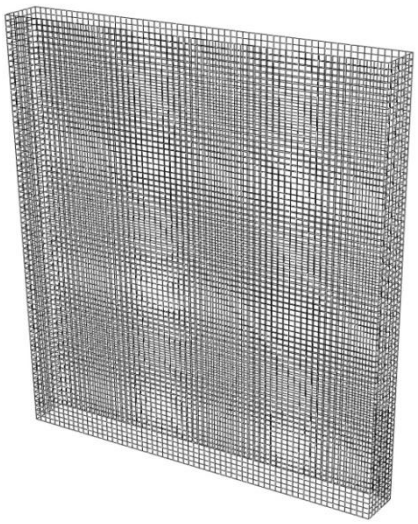

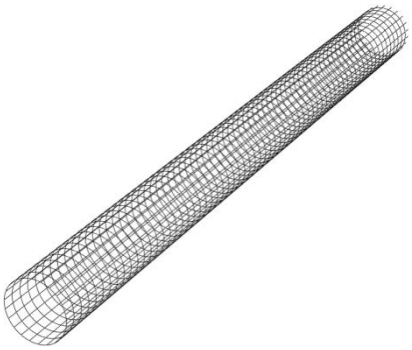

Modeling of welded wire mesh part

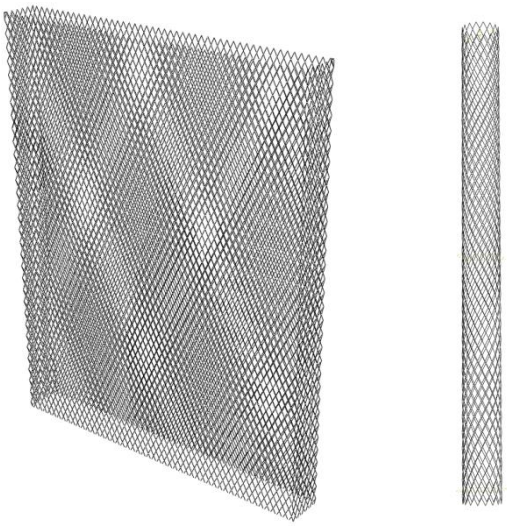

Modeling of expanded mesh part

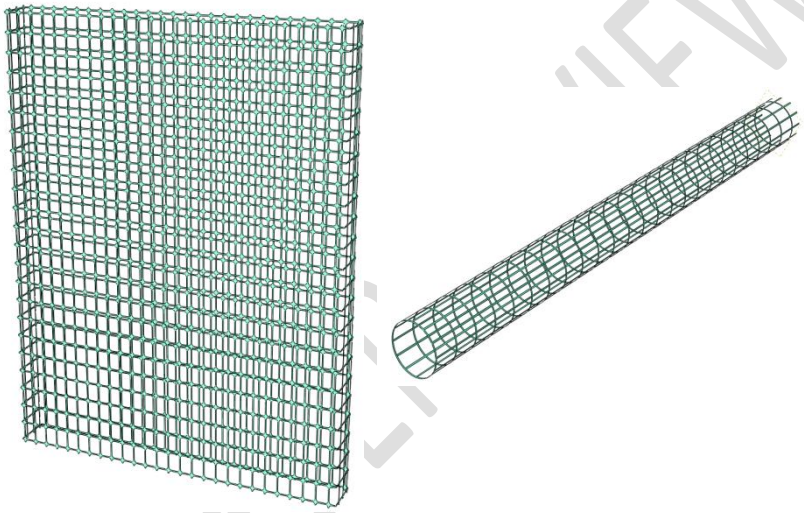

Modeling of tenax mesh part

Fig. (25) Modeling of all parts of the tested specimens.

Materials modeling

Concrete material was modeled using Abaqus concrete damage plasticity model. This model uses the concept of isotropic damage elasticity in combination with isotropic compression and tensile plasticity to model the inelastic behavior of concrete. Tables VII and VIII present concrete elastic properties and concrete damaged plasticity model parameter used in analysis.

Table (10): Elastic properties of concrete.

Parameter	Value
Density	2.2×10^{-9} N/mm3
Modulus oMod of elasticity (Es)	26031 MPa
Poisson's ratio (υ)	0.2

Table (11): Concrete plasticity parameters.

Parameter	Value
Dilation angle	41^{o}
Eccentricity	0.12
fb_0/fc_0	1.36
K	0.68
Viscosity parameter	0.00001
Yield stress in compression	17.493 MPa
inelastic strain	0.0
Compressive ultimate stress	35.086 MPa
Cross bonding inelastic strain	0.00158
Tensile failure stress	3.59 MPa

Steel reinforcement has approximately linear elastic behavior when the steel stiffness introduced by the Young's or elastic modulus keeps constant at low strain magnitudes. At higher strain magnitudes, it begins to have nonlinear, inelastic behavior, which is referred to as plasticity. The plastic behavior of steel is described by its yield point and its post-yield hardening. The shift from elastic to plastic behavior occurs at a yield point on a material stress-strain curve. Table (12) shows the elastic properties of steel bars and metal mesh.

Table (12): The elastic properties of steel bars and metal meshes.

Steel 24/35		**Steel 36/52**		**Welded mesh**		**Expanded mesh**	
Density		**Density**		**Density**		**Density**	
7.86×10^{-9}		7.86×10^{-9}		7.86×10^{-9}		7.8×10^{-9}	
E	**Poisson's ratio**	**E**	**Poisson's ratio**	**E**	**Poisson's ratio**	**E**	**Poisson's ratio**
205000	0.3	210000	0.3	170000	0.28	130000	0.28
stress	**strain**	**stress**	**strain**	**stress**	**strain**	**stress**	**strain**
240	0	570	0	413	0.00	199	0
350	0.0951	730	0.0831	610	0.05763	320	4.95E-02

Tenax mesh was modeled as biaxial Lumina material which has equivalent stress in both main directions (transverse and longitudinal directions) and also has the same fail stress in both directions so it has isotropic and linear behavior only. Table (13) shows the properties of tenax.

Table (13): the properties of tenax

Density	1.02E+02
E	161.5
Poisson's ratio	0.2
Tensile strength , Mpa	9.47E+01
Aperture size MD	4.00E+01
Aperture size TD	2.70E+01
Thickness	2.4

Steel bars, metal meshes and tenax were modeled as embedded region in the surrounding solid elements in the concrete wall as shown in Fig. (26).

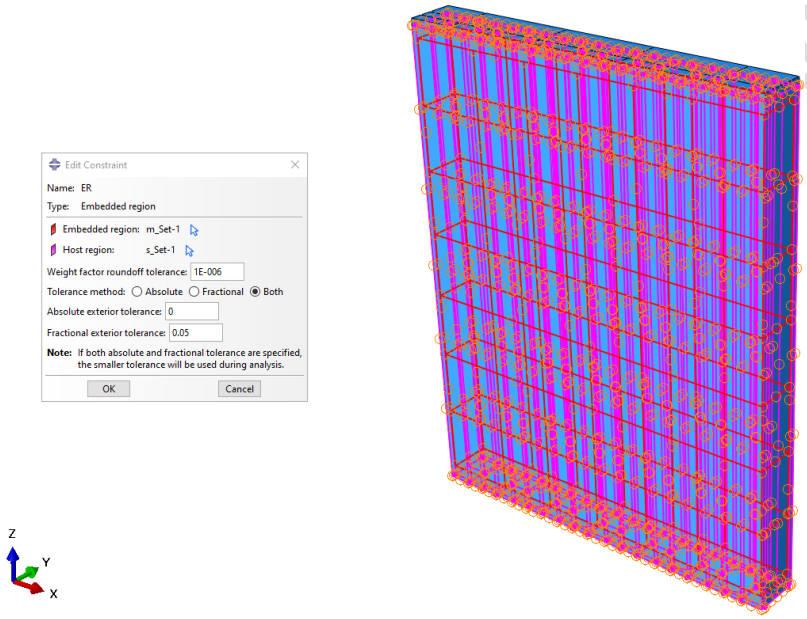

Fig.(26): Interaction.

The loads were modeled as pressure on contact area for specimen. Loads and boundary conditions were illustrated in Fig.(27&28) respectively.

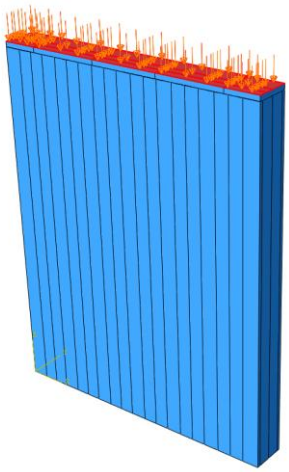

Fig. (27): loading on specimen

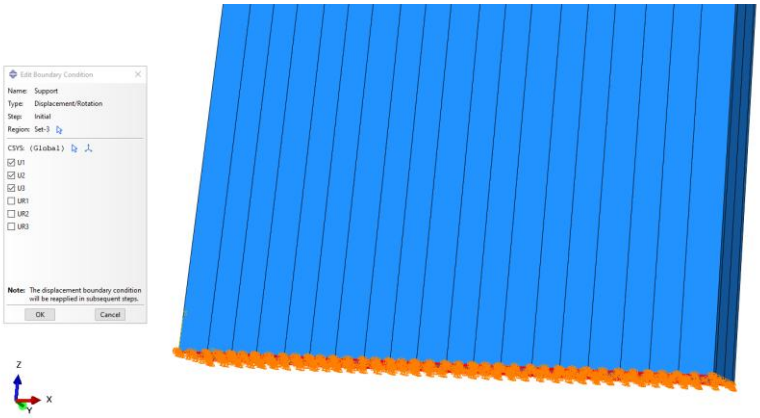

. **Fig. (28):** Boundary condition of model and loads

The models were divided into fine elements with different sizes to allow quick analysis with sufficient accuracy as shown in Fig. (29).

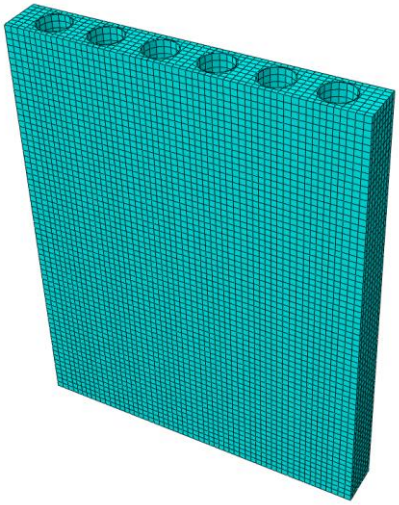

Fig. (29): Meshing of model parts.

Cracking patterns for all tested specimens from the theoretical study

Cracks propagation and modes of failure for each specimen from the theoretical study were recorded as shown in Fig.(29).

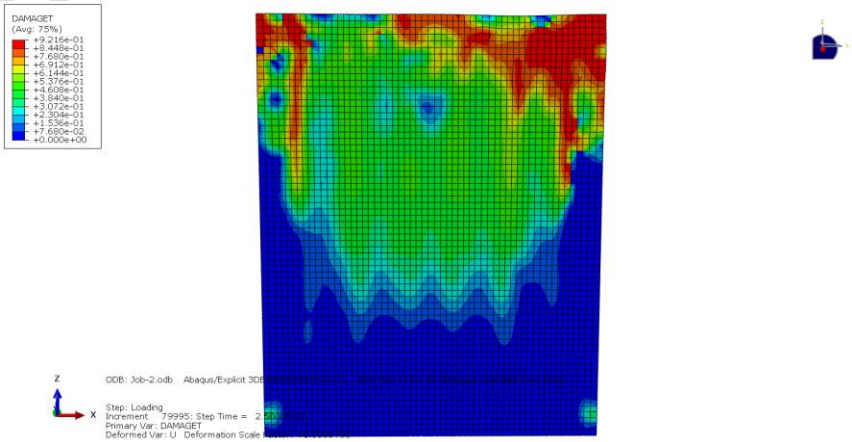

CO specimen

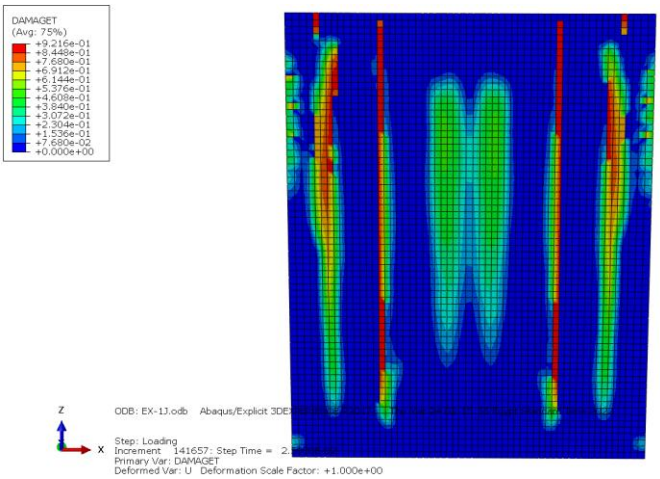

EX1 specimen

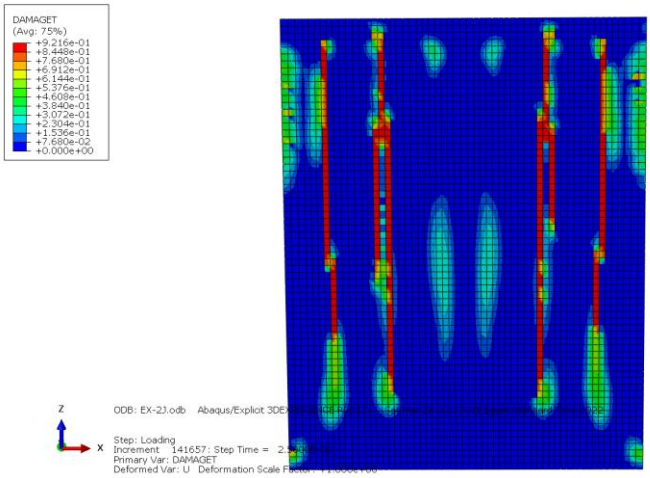

EX2 specimen

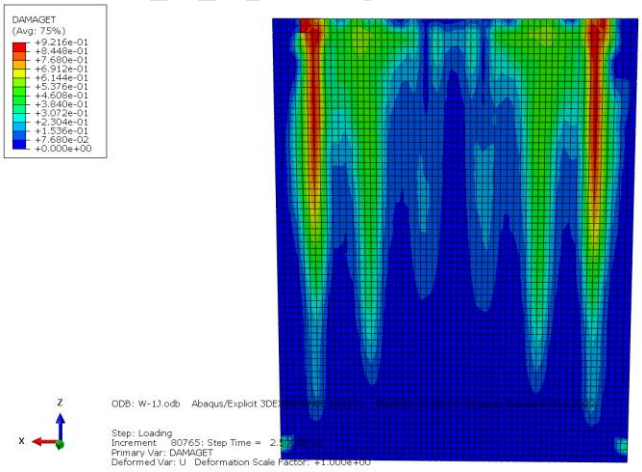

W1 specimen

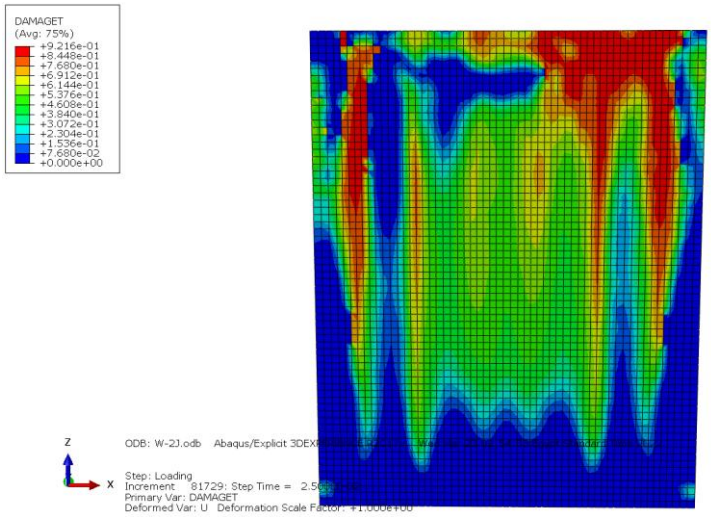

W2 specimen

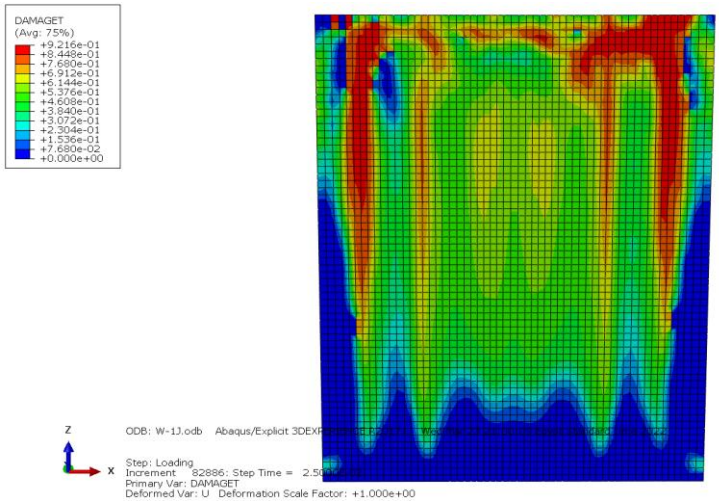

W3 specimen

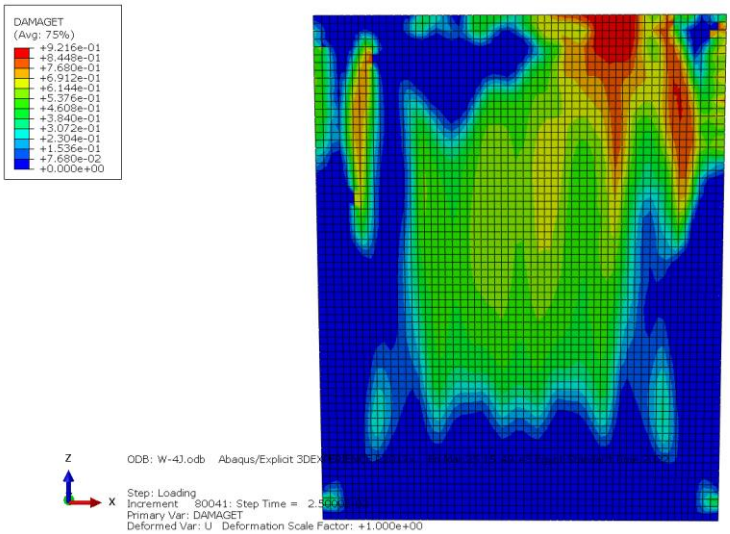

W4 specimen

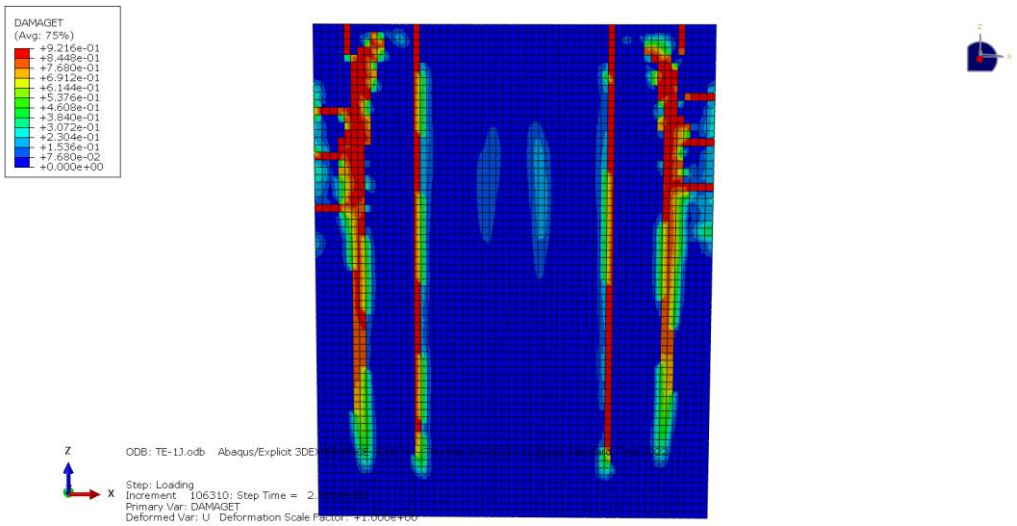

TE1 specimen

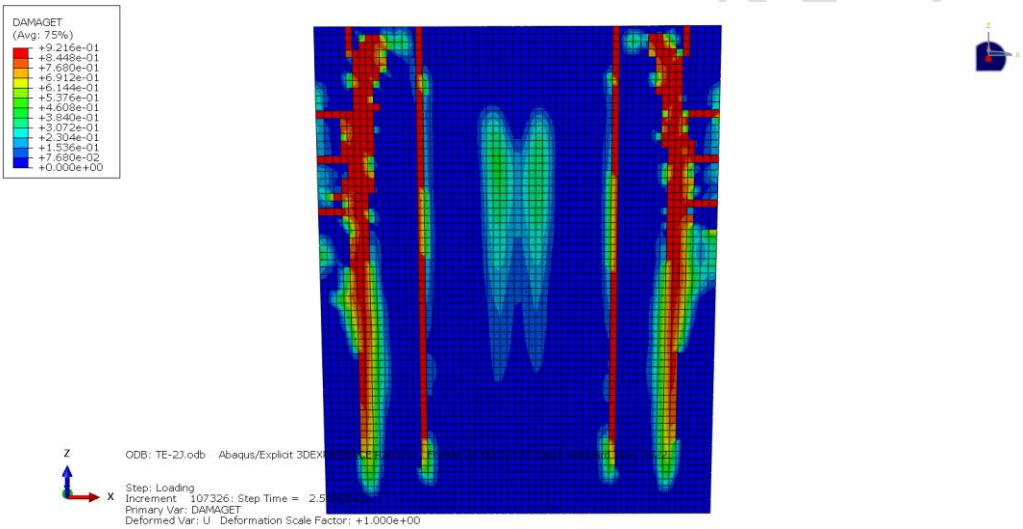

TE2 specimen

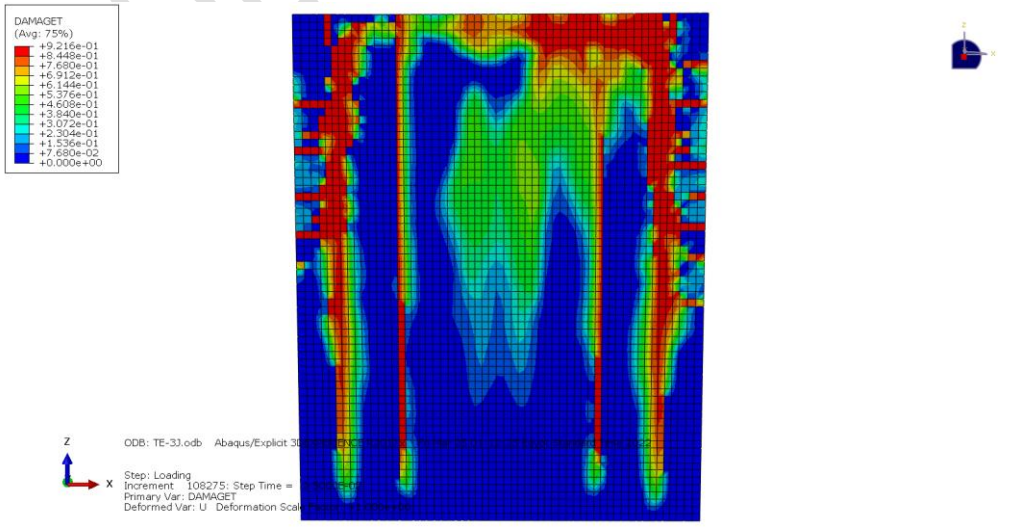

TE3 specimen

Fig.(30): Cracks propagation and modes of failure for each specimen from the theoretical study

Comparison between experimental and finite element simulation results

The experimental results and the numerical results were compared and discussed. As a result, it can be concluded that the finite element simulation gives accurate results when compared with experimental results.

Comparison of the first crack loads and ultimate Loads

Table (14) shows a comparison between experimental results and finite element (FE) simulation for first crack load, ultimate load and vertical displacement at ultimate load. From this table, it observed that that FE simulation gives accurate results when compared with experimental results. It was observed that the percentage of difference for first crack load was found between 0.980 and 1.099 and from 0.889 to 1.10 for ultimate load .however, the percentage of difference for maximum vertical displacement was found between 0.947 to 1.046 as shown in table (14).

Table (14): Comparison between the experimental and theoretical results.

Code of specimen	First Crack load (KN)			Ultimate Load (KN)			Maximum displacement (mm)		
	Finite element method results	Experimental study results	Percentage of difference	Finite element method results	Experimental study results	Percentage of difference	Finite element method results	Experimental study results	Percentage of difference
CO	1774.7	1725.8	1.028	1862.5	1814.6	1.026	1.872	1.788	1.046
W1	1040.1	946.05	1.099	1202.4	1092.9	1.10	1.597	1.534	1.041
W2	1046.6	991.16	1.056	1433.6	1320.9	1.085	2.223	2.299	0.966
W3	1229.5	1132.2	1.085	1639.3	1542.7	1.062	2.493	2.446	1.019
W4	1350.2	1276.1	1.058	1849.5	1771.2	1.044	2.533	2.574	0.984
EX1	920.8	916.3	1.004	1282.4	1298.1	0.987	1.691	1.764	0.958
EX2	1183.6	1120.5	1.056	1582.4	1475.9	1.072	1.852	1.844	1.004
TE1	762.9	723.7	1.054	1125.4	1279.6	0.889	1.677	1.769	0.947
TE2	867.6	884.8	0.980	1266.7	1374.4	0.921	2.069	1.984	1.042
TE3	904.6	920.2	0.983	1320.5	1409.2	0.937	2.727	2.786	0.978

Comparison of Load-Deflection Curves

Fig. (30) shows a comparison of load- deflection curves for all tested specimens as show below.

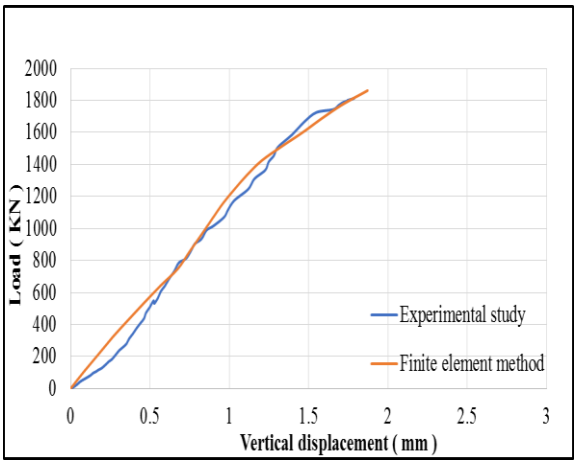

.

(CO) specimen

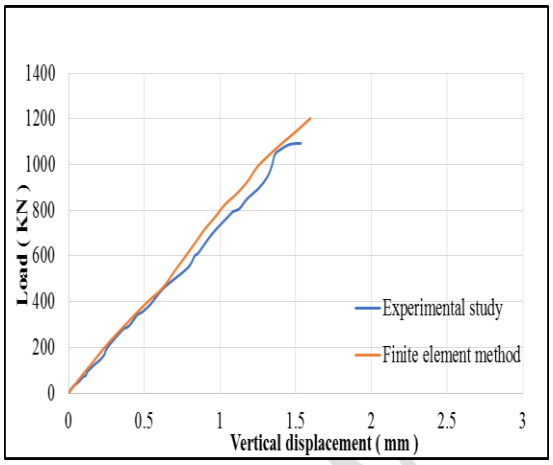

(W1) specimen

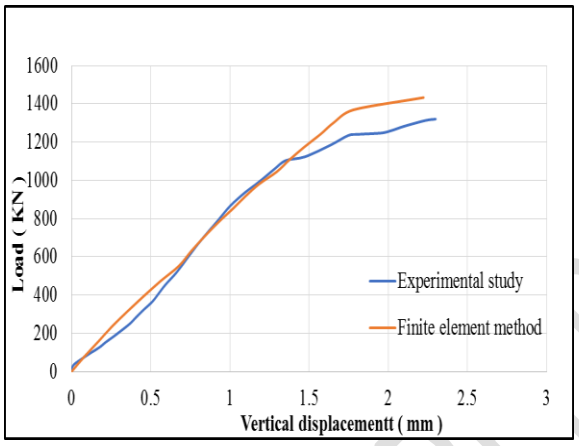

(W2) specimen

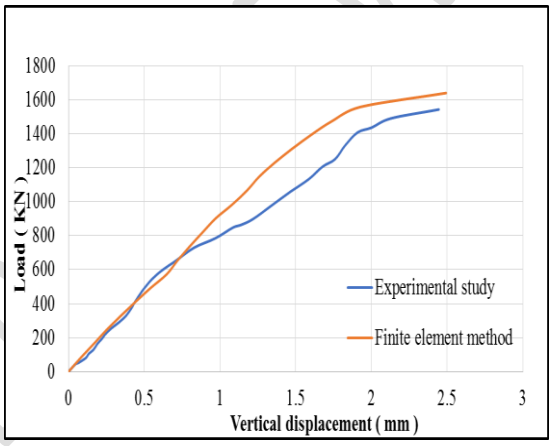

(W3) specimen

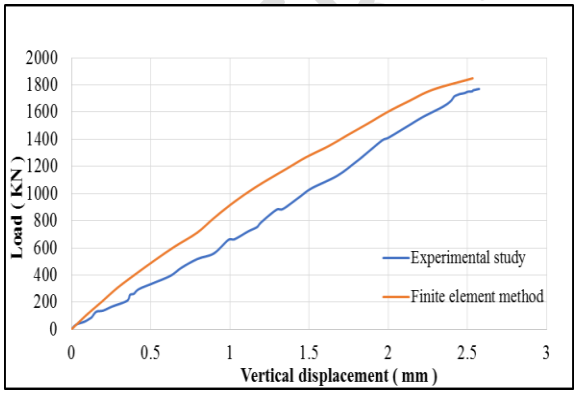

(W4) specimen

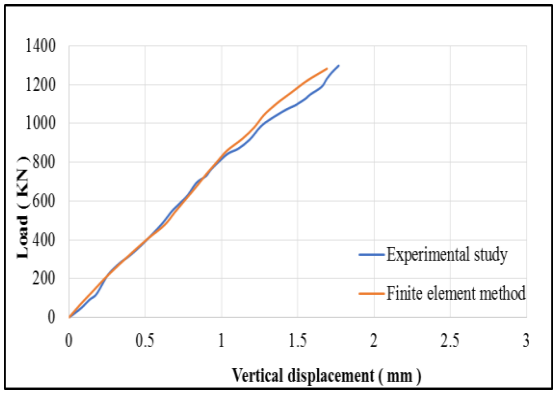

(EX1) specimen

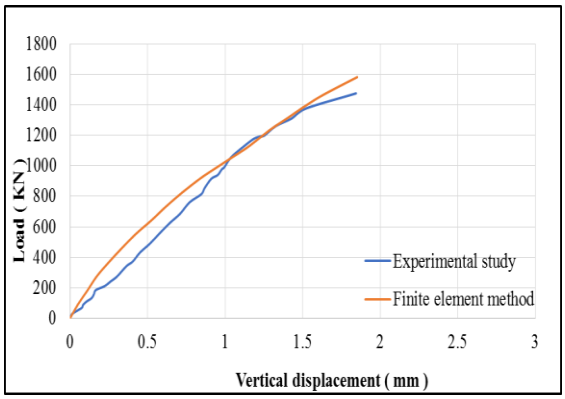

(EX2) specimen

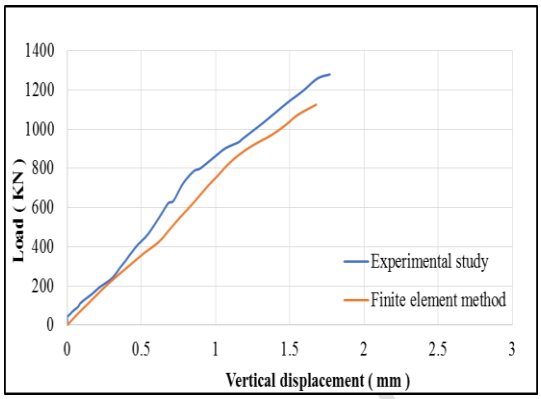

(TE1) specimen

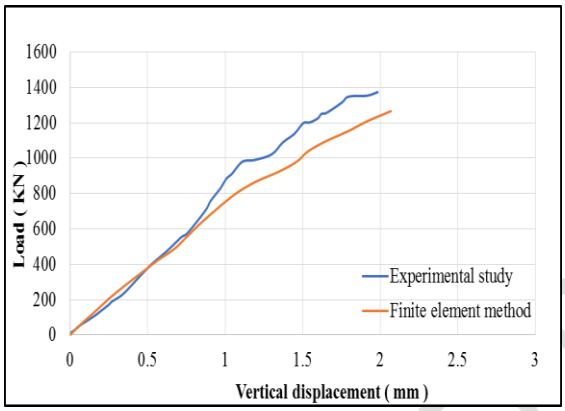

(TE2) specimen

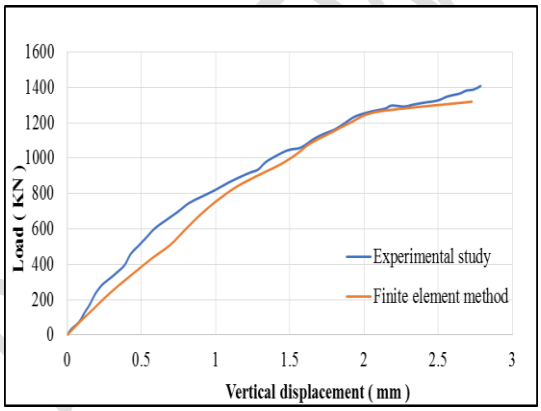

(TE3) specimen

Fig. (31): Load-vertical displacement curves for all tested specimens

Comparison of cracking behavior for (EX1) as an example

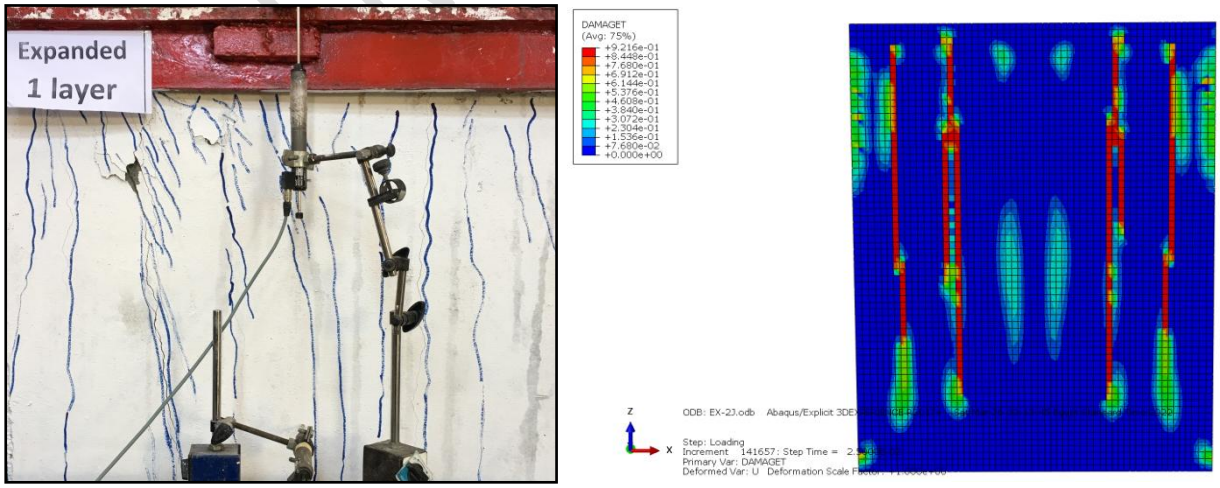

Fig. (32): Experimental and analytical crack patterns (EX1) specimen.

Conclusions

The general conclusions that were extracted from this research work could be drawn as follow:

1- The ultimate load for (CO) specimen was more than the ultimate load for the specimens (W1 , W2 , W3 , W4) and the percentage of increasing was 39.7 % , 27.2 % , 14.9% and 2.4% respectively and the ultimate load for specimen (W4) was more than that of the (W1, W2 , W3) specimens by 38.2% , 25.4 % and 12.9 % respectively.

2- The ultimate load for (CO) specimen was more than the ultimate load for the specimens EX1 and EX2 and the percentage of increasing was 28.4 % and 18.6 % respectively and the ultimate load for specimen (EX2) was more than that of the (EX1) specimen by 12 %.

3- The ultimate load for (CO) specimen was more than the ultimate load for the specimens (T1, T2, T3) by 29.5 %, 24.2 % and 22.3 % respectively and the ultimate load for specimen (T3) was more than that of specimen (T1 and T2) and the percentage of increasing was 9.2 % and 2.4 % respectively.

4- Using one layer expanded steel mesh EX1 was greater than specimens that reinforced with one layer welded wire mesh W1 and one layer tenax mesh TE1 and the percentage of increasing was 15.8% and 1.4% respectively.

5- Using two layers of expanded steel mesh EX2 was greater than specimens that reinforced with two layers of welded wire mesh W2 and two layers of tenax mesh TE2 and the percentage of increasing in ultimate load was 10.5% and 6.9% respectively.

6- The maximum weight/ load ratio for (CO) and (W4) specimens and the minimum weight/ load ratio for (W1) specimen.

7- Increasing the number of the steel mesh layers in the ferrocement forms increases the first crack load, service load, ultimate load, and energy absorption.

8- There is a great saving of weight by making voids area in the cross section of walls leading to easy construction, fire resistance, high sound and thermal isolation.

9- A numerical finite element model can be used to investigate structural characteristics of lightweight ferrocement walls, leading to a good agreement when compared to experimental results.

References

1. Shaheen, Y. B., Z.A. Etman and A.G. Ramadan (2016) "Characteristics of Ferrocement Light Weight Walls", International Journal of Civil Engineering, Springer, Vol. 1, Issue 9.2016, pp.1- 13.

2. Noor A. M., Salihuddin R. S. and Mahyuddin R.(2006), "Strength and Behaviour of Lightweight Ferrocement -Aerated Concrete Sandwich Blocks" Malaysian Journal of Civil Engineering, (2006), 18(2): 99-108.

3. Shaheen, Y. B., Soliman, N.M. and Kotb, H.A.. (2015) " Flexural Behavior of Lightweight Composite Ferrocement Plates", Concrete Research Letters , Vol. 6 (2) – June 2015.

4. Tawab AA, Fahmy EH, Shaheen YB (2012) Use of permanent ferrocement forms for concrete beam construction. Mater Struct 45(9):1319–1329.

5. Shaheen, Y., Eltaly, B. and Abdul-Fataha, S. (2021), "Performance of Ferrocement Box Shear Wall with Webs", International Conference on Advances in Structural and Geotechnical Engineering, ICASGE'21.

6. Shaheen, Y. B. , Fahmy, E.H., and Gaafar, H.M. (2004) " Ferrocement sandwich and hollow core panels for floor construction", Singapore Concrete Institute, 29th Conference on our world in concrete and structures, 25 - 26 August 2004, Singapore.

7. Mahmoud A. E.-W. and Kimio F. (2010), "Flexural Behavior of Lightweight Ferrocement Sandwich Composite Beams" Journal of Science& Technology, 2010, Vol. (15), No. (1), JST (3).

8. Shaheen Y.B., Safan M.A., Abdalla M (2012), "Structural Behavior of Composite Reinforced Ferrocement Plates" Concrete Research Letters, Sept. 2012, Vol. 3.

9. Abaqus User's Guide, Abaqus Documentation User's Guide. s.l.:Dassault Systèmes, Simulia Corp, 2013.

10. Shaheen, Y. B. and R.N. Swamy (1990) "Tensile Behaviour of thin Ferrocement plates " A C I, SP-124, September 1990, PP 357-387.

11. I.A. Basunbul, M. Saleem, and G.J. Al-Sulaimani, (1990) "Structural Behavior of Ferrocement Load Bearing Wall Panels", Journal of Ferrocement: Vol. 20, No. 1, January 1990, pp 1-9.

12. ACI 549R-97 (1993), State-of-the-Art Report on Ferrocement, American Concrete Institute, Detroit, MI 48219, USA 7.

13. W.N. Al-Rifiaie and A.A. Aziz (1995) "Thin Ferrocement Bearing Walls" , Journal of Ferrocement: Vol. 25, No. 3, July 1995, pp 247-259.

14. ACI Committee 549 (1997) State-of-the-Art report on ferrocement. ACI549-R97, in manual of concrete practice. ACI, Detroit, p 26.

15. Shaheen, Y. B., E.H. Fahmy and Y.S. Korany (1999) "Repairing Reinforced Concrete Columns Using Ferrocement Laminates", Journal of Ferrocement: Vol. 29, No. 2, April 1999, pp. 115-124.

16. Naaman AE (2000) Ferrocement and laminated cementitious composites. Materials and structures, vol 33, No. 1. Techno Press, Ann Arbor 4.

17. Takiguchi K & Abdullah, (2001), “Shear Strengthening of Reinforced Concrete Columns using Ferrocement Jackets”. ACI Structural Journal, 98(5): 696–704

18. Wang S, Naaman AE, Li VC (2004) Bending response of hybrid ferrocement plates with meshes and fibers. J Ferrocem 34(1):275–288.

19. Greepala V, Nimityongskul P (2006) Structural integrity and insulation property of ferrocement exposed to fire. In: 8th International symposium and workshop on ferrocement and thin reinforced cement composites bangkok, Thailand, February 6–8, 2006.

20. Gaba H, Singh H (2008) The study of economy of ferrocement with flyash as an admixture. In: 12th international conference of international association for computer methods and advances in geomechanics (IACMAG), pp 1–6.

21. Eltehawy E (2009) Effect of using ferro-cement on the mechanical properties of reinforced concrete slabs subjected to dynamic loads. In: 13th international conference on aerospace science and aviation technology (ASAT), pp 1–13.

22. Xiong, G., Wu, X., Li, F., and Yan, Z. (2011) “Load carrying capacity and ductility of circular concrete columns confined by ferrocement including steel bars” Construction and Building Materials, Vol. 25, PP. 2263–2268, 2011.

23. Sasiekalaa K, Malathy R (2012) A review on mechanical properties of ferrocement with cementitious materials. Int J Eng Res Technol 1(9):1–20 9.

24. Shaheen, Y. B. , Fahmy, E.H., and Gaafar, H.M. (2012) " Ferrocement sandwich and hollow core panels for floor construction", Canadian Journal of Civil Engineering • 26 October 2012, Vol.39.

25. Kaish, A., Alam, M., Jamil, M., Zain, M., and Wahed, M. (2012) "Improved ferrocement jacketing for strengthening of square RC short column" Construction and Building Materials, Vol. 36, PP. 228–237, .2012.

26. Mourad, S.M., and Shannag, M.J. (2012) "Repair and strengthening of reinforced concrete square columns using ferrocement jackets" Cement and Concrete Composites, Vol.34, PP. 288–294, 2012.

27. Shaheen, Y. B., Soliman,N.M. and Hafez,A.M, (2013) " Structural Behaviour of Ferrocement channels Beams", Concrete research letters, Vol. 4 (3) –Sept. 2013.

28. Shaheen, Y. B. , R.M. Abd El-Naby, M.A.Adam and A.M. Erfan (2014) " Strength And Behavior of Innovative Composite Columns" international Journal of Civil Engineering and Technology (IJCIET),Volume 5, November (2014), Pp.125-145.

29. Shaheen, Y., Eltaly, B. and Abdul-Fataha, S. (2014), "Structural performance of ferrocement beams reinforced with composite materials", Struct. Eng. Mech., 50(6), 817-834.

30. Shaheen, Y. B., Naser,A.A. and Elhabashy,W.S. (2014) " Shear behavior of light weight ferrocement concrete slabs", ERJ. Engineering research journal, Volume 37, Issue 4, October 2014.

31. S.Sirimontree, B.Witchayangkoon and K.Lertpocasombubut (2015) "Strengthening of Reinforced Concrete Column via Ferrocement Jacketing", Construction Innovation, Vol. 4, No. 1, 2015. Pp.39-47.

32. Shaheen, Y. B., Ashraf.M. Amin, H.M. Refaat (2017) "Experimental and FE simulations of ferrocement columns incorporating composite materials" Structural and Engineering Mechanics, Vol. 64, No. 2, 2017. Pp.155-171.

33. Shaheen, Y. B. and Eltehawy, E. A. (2017). Structural behaviour of ferrocement channels slabs for low cost housing. Challenge J. Concr. Res. Lett, 8(2), 48-64.

34. Shaheen, Y. B. , Z.A. Etman, and A.G. Ramadan (2018) "Characteristics of ferrocement lightweight wall", International Concrete and Computer Journal" 16(1), 33-45, 2018.

35. M.H. Rashid, Z Alam, and F.J. Mahmud, and M.S. Anita (2019) "Durability and Performance of Ferrocement Infill Wall Panel ", Journal of Ferrocement: Vol. 5, No. 6, June 2019, pp 1205- 1213.

36. Ramakrishnan, K., Muthu, D., & Viveka, S. (2020). An Experimental Investigation of Flexural Behaviour of Ferrocement Box Beams Using Micro Fillers. In Sustainable Practices and Innovations in Civil Engineering (pp. 87-96).

37. Abbass, A. A., Abid, S. R., Arna'ot, F. H., Al-Ameri, R. A. and Özakça, M. (2020). Flexural response of hollow high strength concrete beams considering different size reductions. In Structures (Vol. 23, pp. 69-86).

38. Naser, F. H., Al Mamoori, A. H. N., & Dhahir, M. K. (2020). Effect of using different types of reinforcement on the flexural behavior of ferrocement hollow core slabs embedding PVC pipes. Ain Shams Engineering Journal.

39. Du, W., Yang, C., Wang, C., Pan, Y., Zhang, H., & Yuan, W. (2021). Flexural Behavior of Polyvinyl Alcohol Fiber–Reinforced Ferrocement Cementitious Composite. Journal of Materials in Civil Engineering, 33(4), 04021040.